Cellular Microbiology (2015) **17**(12), 1848–1867
doi:10.1111/cmi.12477
First published online 24 July 2015

A *Plasmodium* α/β-hydrolase modulates the development of invasive stages

Anna M. Groat-Carmona,[1] Heather Kain,[1] Jessica Brownell,[1] Alyse N. Douglass,[1] Ahmed S. I. Aly[2] and Stefan H. I. Kappe[1,3]*
[1]*Center for Infectious Disease Research, formerly Seattle BioMedical Research Institute, Seattle, WA, USA.*
[2]*School of Public Health and Tropical Medicine, Tulane University, New Orleans, LA, USA.*
[3]*Department of Global Health, University of Washington, Seattle, WA, USA.*

Summary

The bud emergence (BEM)46 proteins are evolutionarily conserved members of the α/β-hydrolase superfamily, which includes enzymes with diverse functions and a wide range of substrates. Here, we identified a *Plasmodium* BEM46-like protein (PBLP) and characterized it throughout the life cycle of the rodent malaria parasite *Plasmodium yoelii.* The *Plasmodium* BEM46-like protein is shown to be closely associated with the parasite plasma membrane of asexual erythrocytic stage schizonts and exo-erythrocytic schizonts; however, PBLP localizes to unique intracellular structures in sporozoites. Generation and analysis of *P. yoelii* knockout (Δ*pblp*) parasite lines showed that PBLP has an important role in erythrocytic stage merozoite development with Δ*pblp* parasites forming fewer merozoites during schizogony, which results in decreased parasitemia when compared with wild-type (WT) parasites. Δ*pblp* parasites showed no defects in gametogenesis or transmission to mosquitoes; however, because they formed fewer oocysts there was a reduction in the number of developed sporozoites in infected mosquitoes when compared with WT. Although Δ*pblp* sporozoites showed no apparent defect in mosquito salivary gland infection, they showed decreased infectivity in hepatocytes *in vitro.* Similarly, mice infected with Δ*pblp* sporozoites exhibited a delay in the onset of blood-stage patency, which is likely caused by reduced sporozoite infectivity and a discernible delay in exo-erythrocytic merozoite formation. These data are consistent with the model that PBLP has an important role in parasite invasive-stage morphogenesis throughout the parasite life cycle.

Received 13 January, 2015; revised 19 June, 2015; accepted 23 June, 2015. *For correspondence. E-mail stefan.kappe@cidresearch.org; Tel. (+1) 206 256 7205; Fax (+1) 206 256 7229.

Introduction

Malaria parasites are obligatory intracellular protists in the genus *Plasmodium* that are transmitted by Anopheline mosquitoes, continuously cycling their residence between their insect vectors and mammalian hosts. Within each, the parasite undergoes extensive growth and development to produce invasive forms, which allows it to disseminate and ensure life cycle progression. Female *Anopheles* mosquitoes ingest the sexual stages of the parasite when they take a blood meal, which mate to form a zygote that transforms into a motile ookinete and invades the mosquito midgut epithelium to form a sessile oocyst that grows and matures within a few weeks to produce thousands of sporozoites. These are subsequently released into the haemocoel of the mosquito and invade the salivary glands, where they accumulate and become highly motile and infectious. A few hundred sporozoites are then deposited into the skin by an infected mosquito during a blood meal (Jin *et al.*, 2007), enter the bloodstream by means of active locomotion and are transported to the liver to infect hepatocytes (Vanderberg and Frevert, 2004; Amino *et al.*, 2006). Intracellular sporozoites become liver-stage (LS) parasites, which grow and differentiate in order to produce up to 40 000 infectious exo-erythrocytic merozoites (Shortt *et al.*, 1951; Meis *et al.*, 1983; Prudencio *et al.*, 2006; Sturm *et al.*, 2006) that will undergo multiple rounds of intra-erythrocytic growth. While liver infections do not result in overt pathology, they do lead to a massive one-time amplification of parasite numbers (Vaughan *et al.*, 2008) whereas replication within infected red blood cells (iRBCs) is cyclic and produces up to a few dozen merozoites after each invasive cycle (Cowman and Crabb, 2006), resulting in malaria-associated pathology. The *Plasmodium* life cycle is completed when a small percentage of merozoites develop into the male and female gametocytes, which can be taken up by mosquitoes during subsequent blood meals.

During blood-stage (BS) schizogony, a single invading merozoite transforms into a trophozoite and undergoes rounds of nuclear and organelle replication to form a syncytial schizont with 16–22 nuclei (Read *et al.*, 1993; Arnot and Gull, 1998; Bannister *et al.*, 2000; Margos *et al.*, 2004), which differentiate into individual merozoites. However, during oocyst development, a series of nuclear and organelle replication steps in a syncytium (sporoblast) produce several thousand copies of each within the oocyst (Sinden, 1999; Stanway *et al.*, 2011) although it is only in the final phase of growth that individual sporozoites emerge by budding off the oocyst surface (Rosenberg and Rungsiwongse, 1991; Schrevel *et al.*, 2008). Breakdown of the oocyst capsule subsequently release sporozoites into the haemocoel (Aly and Matuschewski, 2005), particularly the thorax (Golenda *et al.*, 1990) but only ~20% of sporozoites successfully invade the salivary glands (Rosenberg and Rungsiwongse, 1991). During exo-erythrocytic schizogony, a single invading sporozoite de-differentiates into a trophozoite before undergoing extensive mitotic division without cytokinesis to form a multinucleated schizont (Meis *et al.*, 1990). The syncytial schizont later undergoes extensive invagination of its plasma membrane, from which tens of thousands of exo-erythrocytic merozoites (Shortt *et al.*, 1951; Bray and Garnham, 1982) are formed. These are eventually released into the bloodstream in parasite-filled vesicles, called merosomes (Sturm *et al.*, 2006). Despite the fact that schizogony and sporogony are critical parasite amplification events, little is known about the molecular factors that control these unique forms of replication and the universal regulators that modulate them have not been characterized.

In this study, we examine an as of yet uncharacterized *Plasmodium* BEM46-like protein (PBLP) that appears to have a global role in modulating maturation of the invasive stages, spanning all replication stages of the parasite life cycle. All eukaryotic organisms carry a homologue of the bud emergence (BEM)46 protein (Valencik and Pringle, 1995; Mochizuki *et al.*, 2005), which possesses a conserved amino acid motif in the α/β-hydrolase superfamily that includes enzymes with diverse functions and a wide range of substrates (Ollis *et al.*, 1992; Holmquist, 2000). Although the biochemistry of these family members is well described, few members of the α/β-hydrolase superfamily have known biological functions although BEM46 homologues have been implicated in playing a role in broad cellular functions such as signal transduction and cell polarity in order to affect cell morphogenesis at the cell surface (Valencik and Pringle, 1995; Cabib *et al.*, 1998; Madden and Snyder, 1998; Mercker *et al.*, 2009). We examined the role of PBLP throughout the *Plasmodium yoelii* life cycle and determined that this protein is constitutively expressed and has an important role in intra-erythrocytic and exo-erythrocytic stage merozoite development as well as oocyst formation and sporozoite maturation. The identification of parasite proteins that modulate invasive-stage formation throughout the life cycle will provide a conduit by which to gain insights into the molecular mechanisms underlying the unique cell morphogenesis of malaria parasites during schizogony and sporogony.

Results

A BEM46 orthologue is constitutively expressed throughout the P. yoelii *life cycle and is conserved in all* Plasmodium *spp.*

Recent investigations into differential gene expression patterns in *Plasmodium* oocyst- and salivary gland-derived sporozoites (sgSpz) led to the identification of the *PBLP* gene, which encodes a small single transmembrane protein within 11 exons (Supporting Information Fig. S1) (Lindner *et al.*, 2013a,b). Interestingly, PBLP was also observed in the LS transcriptome and proteome at 40 h post infection (Tarun *et al.*, 2008). To establish the expression pattern of *PBLP* transcripts *in vivo*, we analysed *PBLP* mRNA levels in *P. yoelii* 17XNL wild-type (WT) sgSpz isolated from *Anopheles stephensi* mosquitoes, BS parasites or in livers of infected mice at 24 and 45 hours post sporozoite infection (hpi) (Fig. 1A). Amplification of parasite 18S ribosomal RNA (rRNA) was used as a positive control (Fig. 1A). *Plasmodium* BEM46-like protein transcripts were detected in all tested samples, indicating that the gene is constitutively expressed (Fig. 1A).

The *Plasmodium* BEM46-like protein is conserved across *Plasmodium* spp., sharing structural homology and amino acid identity with BEM46-like proteins in the α/β-hydrolase superfamily (Table 1). Like other BEM46 members, the protein encodes a signal peptide that could act as a putative transmembrane domain at the N-terminus and an α/β-hydrolase domain at the C-terminus, the latter of which is common to several hydrolytic enzymes with diverse catalytic functions (Nardini and Dijkstra, 1999) (Fig. 1B). While all eukaryotic organisms are reported to carry a homologue of the BEM46 protein (Valencik and Pringle, 1995; Mochizuki *et al.*, 2005), they have only been characterized in *Schizosaccharomyces pombe*, *Saccharomyces cerevisiae*, *Neurospora crassa*, *Drosophila melanogaster*, *Arabidopsis thaliana*, *Aspergillus nidulans* and *Mus musculus* (Table 1). Overall, the molecular function of most BEM46 proteins remains unknown and the majority of their substrates have not been identified. Additional BLAST searches in the *P. yoelii* 17XNL genome revealed the presence of a number of additional putative BEM46 proteins, none of which have been characterized to date (Supporting Information Table S1). Additionally, all *Plasmodium* spp. appear to contain a PBLP orthologue, which suggests a conserved function across *Plasmodium* species (Fig. 1C).

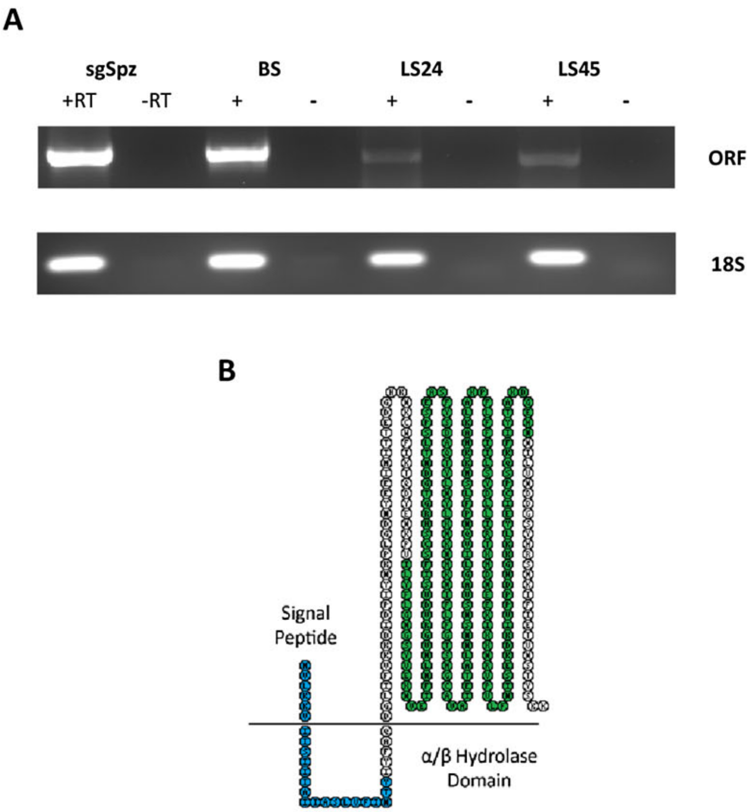

C

```
PY17XNL     MVLKKVIISIIIAIIASLVFINTYIYFAQDGLIFVKKDIDP-IYNKPLGDNYEEIMITTE 59
PF3D7       MRIIKYIFFAFIIILALFVCALNTYIYLKQDSFVFSNEFPTVEEKNQTLGENYEIVTLTTK 60
            * : * *:  :* :   :  :*****: **.::* ::       *:.**:*** : :**:

PY17XNL     DGHKNKCWFIKTQDYENKPVILYFLGNGSYVEKNVEIFNLMVGRVDVSIFSCSHRGTGDN 119
PF3D7       DNHKFTCWYIKTKDSENKPIMLYFQGNGGYLEKYMNLFNLIIERVDVNIFSCSNRGCGSN 120
            *.** .**:***:* ****::*** ***.*:** :::***:: ****.*****:** *.*

PY17XNL     TLSPSEASFYSDAQTYLNYLKMKNMKNIFLFGTSMGCAVAIETALNNSNSVAGLIVQNPF 179
PF3D7       IAKPSEEYFYKDAHVYIEYVKTKNPKHLFIFGSSMGAAVAIDTALKQHDHISGLIVQNAF 180
              .***  **.**:.*::*:* ** *::*:**:***.****:***:: : ::******.*

PY17XNL     LSMKKMAKLAKPFLFFIILSYDLLIRTKMDNEEKIKKNRVPVLFNISEKDKIVPPDHGKK 239
PF3D7       TSLKELSRYSHPFLNYFLFDYDMIIRSKMDNETKIKNITVPTLFTLSEMDEKVPTSHTRT 240
             *:*:::: ::*** ::::.**::**:***** ***:  **.**.:** *: **..* :.

PY17XNL     LYEICPSQ-KFIYTAKDGEHNNILVNDDGSYHRSMKIFIETVNSTYSKK----------- 287
PF3D7       LFQLSASTNKQLYLSKGGTHPNILKNDDGSYHKAMKKFIVTAISIREKNIQKAVERNPNT 300
            *:::..*  * :* :*.* * *** *******::** ** *. *  .*:

PY17XNL     --
PF3D7       PN 302
```

Fig. 1. PBLP is a putative member of the BEM46 family that is constitutively expressed in all stages of the *Plasmodium yoelii* life cycle.
A. The *PBLP* transcript is expressed in mixed BS, salivary gland-derived sporozoites (sgSpz) and (LS. PBLP expression was determined by RT-PCR on RNA derived from *P. yoelii* 17XNL salivary gland sporozoites, mixed BS parasites and mouse livers infected with 1×10^6 salivary gland-derived sporozoites (livers were isolated at 24 or 45 h post infection). Genomic DNA was removed by DNase treatment and cDNA was generated by reverse transcriptase PCR (+RT). Either *PBLP* (ORF) or 18S rRNA (18S) was amplified from the synthesized cDNA via 35 cycles of PCR. Non-RT controls (-RT) were included to confirm that PBLP amplification was due to cDNA and not to residual genomic DNA.
B. PBLP displays a predicted protein structure that is characteristic of the BEM46 family of proteins, which all contain an α/β-hydrolase domain. The protein structure prediction was generated using the TOPO2 Transmembrane Protein Display. The putative signal peptide is shown in blue while the characteristic α/β-hydrolase domain is shown in green.
C. PBLP is highly conserved in both mouse and human malaria strains, implying a shared function. The PBLP amino acid sequence from the experimental mouse strain *P. yoelii* 17XNL (PY06542, PY17XNL) and the human strain *P. falciparum* 3D7 (PF3D7_0818600, PF3D7) were aligned using *Clustal Omega*. Positions of complete sequence homology are indicated by asterisks; partial and decreasing levels of homology are indicated by (:) or (.) respectively.

PBLP localizes to the parasite plasma membrane (PPM) in LS and BS parasites

In order to determine the location of PBLP in different stages of the life cycle, we fused a C-terminal quadruple myc tag to the PBLP protein in *P. yoelii*, termed *pblp*-myc (#1 and #2), using a double-crossover recombination strategy (Mikolajczak *et al.*, 2008) (Supporting Information Fig. S2A). The recombinant parasites were cloned by serial dilution and the clonal identity of the parasites (*pblp*-myc tag #1 and #2), derived from two independent transfections, was confirmed by PCR (Supporting Information Fig. S2B). We monitored mRNA expression in mixed iRBCs by reverse transcription PCR (RT-PCR) and as expected, *PBLP* transcripts were detected in each of the *pblp*-myc-tag clones (Supporting Information Fig. S2C).

Mixed iRBCs were isolated from mice infected with *pblp*-myc parasites and cultured *in vitro* for 12 h to generate a homogeneous population of schizonts, which were isolated using an Accudenz density cushion. Isolated schizonts were examined using indirect immunofluorescence assays (IFAs), which showed that that PBLP significantly co-localizes with the merozoite surface protein 1 (MSP-1) in schizont-containing iRBCs, indicating that PBLP could be associated with the PPM in intraerythrocytic merozoites (Fig. 2A). In developing oocysts,

Table 1. Amino acid conservation of the *Plasmodium yoelii* 17XNL PBLP protein in *Plasmodium* spp. (shown in grey) and other known BEM46 proteins within the α/β-hydrolase superfamily.

Organism	Protein product	aa identity (%)	Probability score	Accession code	Known function
Plasmodium berghei	Conserved unknown protein	89	4.20E-141	PBANKA_071220	–
P. vivax	Hypothetical protein	56	6.30E-83	PVX_089485	–
P. knowlesi	Conserved unknown protein	51	1.80E-78	PKH_051320	–
P. falciparum IT	Conserved unknown protein	50	8.00E-76	PFIT_0821500	–
P. falciparum 3D7	Conserved unknown protein	49	7.20E-75	PF3D7_0818600	–
Arabidopsis thaliana	WAV2	32	1.6E-23	AB182157	Modulates root tip bending (Mochizuki *et al.*, 2005)
Oryza sativa	BEM46-like protein	28	9.6E-24	AK106096	– (Mochizuki *et al.*, 2005)
Schizosaccharomyces pombe	*S. cerevisiae bem1/bud5* suppressor	32	3.2E-25	U29892	Involved in cell polarization and budding (Chant *et al.*, 1991; Chenevert *et al.*, 1992; Valencik and Pringle, 1995; Park *et al.*, 1997; Cabib *et al.*, 1998; Madden and Snyder, 1998; Irazoqui *et al.*, 2003)
Saccharomyces cerevisiae	BEM46-like protein (YNL320w)	32	9.6E-24	Z71596	Not essential (Giaever *et al.*, 2002)
Escherichia coli	Uncharacterized protein YfhR	23	3.8E-12	P77538	– (Mochizuki *et al.*, 2005)
Neurospora crassa	BEM46-like protein	28	3.2E-24	Q7SDX9	Required for hyphal growth upon ascospore germination (Mercker *et al.*, 2009)
Drosophila melanogaster	BEM46-like protein (RAPSYNOID)	26	1.1E-18	AF069781	Controls asymmetric cell division (Parmentier *et al.*, 2000; Giot *et al.*, 2003)
Mus musculus	α/β hydrolase domain containing 13	30	1.7E-25	BC043690	– (Mochizuki *et al.*, 2005; Mercker *et al.*, 2009)
Aspergillus nidulans	BemA (BEM1 homologue)	31	1.7E-16	CBF75456	Involved in polarisome formation (Leeder and Tumer, 2008)

PBLP significantly co-localized with the circumsporozoite protein (CSP) (Fig. 2B), which is a PPM-resident protein in fully developed sporozoites. However, PBLP showed a unique intracellular localization in salivary gland-derived *pblp*-myc-tag sporozoites, which did not overlap with the ER marker (BIP, Fig. 2C), the micronemal marker (TRAP, data not shown) or a rhoptry marker (Ron4, data not shown), although it was distinctly vesicular.

In order to track PBLP localization during LS development, *pblp*-myc sporozoites were used to infect BALB/cJ mice. *pblp*-myc-infected livers were isolated at 24 (Fig. 2D), 45 (Fig. 2E) and 52 hpi (Fig. 2F), sectioned and then analysed by IFA. At 24 hpi, PBLP co-localized with CSP, which at this point is still found associated with the PPM of LS parasites (Fig. 2D). During later points of LS development, PBLP co-localized with MSP-1 on the LS surface, clearly decorating the plasma membrane invaginations known as cytomeres (Fig. 2E). In the final stage of exo-erythrocytic schizogony, PBLP continued to co-localize with MSP-1 on the PPM of developed merozoites (Fig. 2F). Since PBLP never co-localized with known parasitophorous vacuole membrane (PVM) proteins (Hep17, Fig. 2A, E and F), these studies support our claim that PBLP co-localizes with the PPM in BS (Fig. 2A) and LS parasites (Fig. 2E and F).

Deletion of PBLP *affects merozoite formation*

To determine the importance of PBLP in the parasite life cycle, we generated two distinct PBLP knockouts (Δ*pblp*) in *P. yoelii*, termed Δ*pblp* version #1 (Δ*pblp* v1) and version #2 (Δ*pblp* v2), using the double-crossover recombination strategy described earlier (Mikolajczak *et al.*, 2008) (Supporting Information Fig. S3A). Δ*pblp* v1 maintained small portions of the open reading frame (ORF) (Supporting Information Fig. S3A, *left panel*) whereas Δ*pblp* v2 carried a complete deletion (Supporting Information Fig. S3A, *right panel*). The α/β-hydrolase domain was absent in both knockouts. Recombinant parasites were cloned by serial dilution and the clonal identity of the two parasite lines (Δ*pblp* v1 and Δ*pblp* v2) was confirmed by PCR (Supporting Information Fig. S3B) while the lack of *PBLP* expression was determined by RT-PCR (Supporting Information Fig. S3C). Since the design of the Δ*pblp* v1 clone resulted in a transcript that was much larger than the predicted WT sequence (Supporting Information Fig. S3C), the complete replacement of the *PBLP* ORF was confirmed by sequencing genomic DNA that was isolated from BS parasites (data not shown).

To test whether deletion of PBLP had an effect on BS development, we injected BALB/cJ mice with 1×10^6

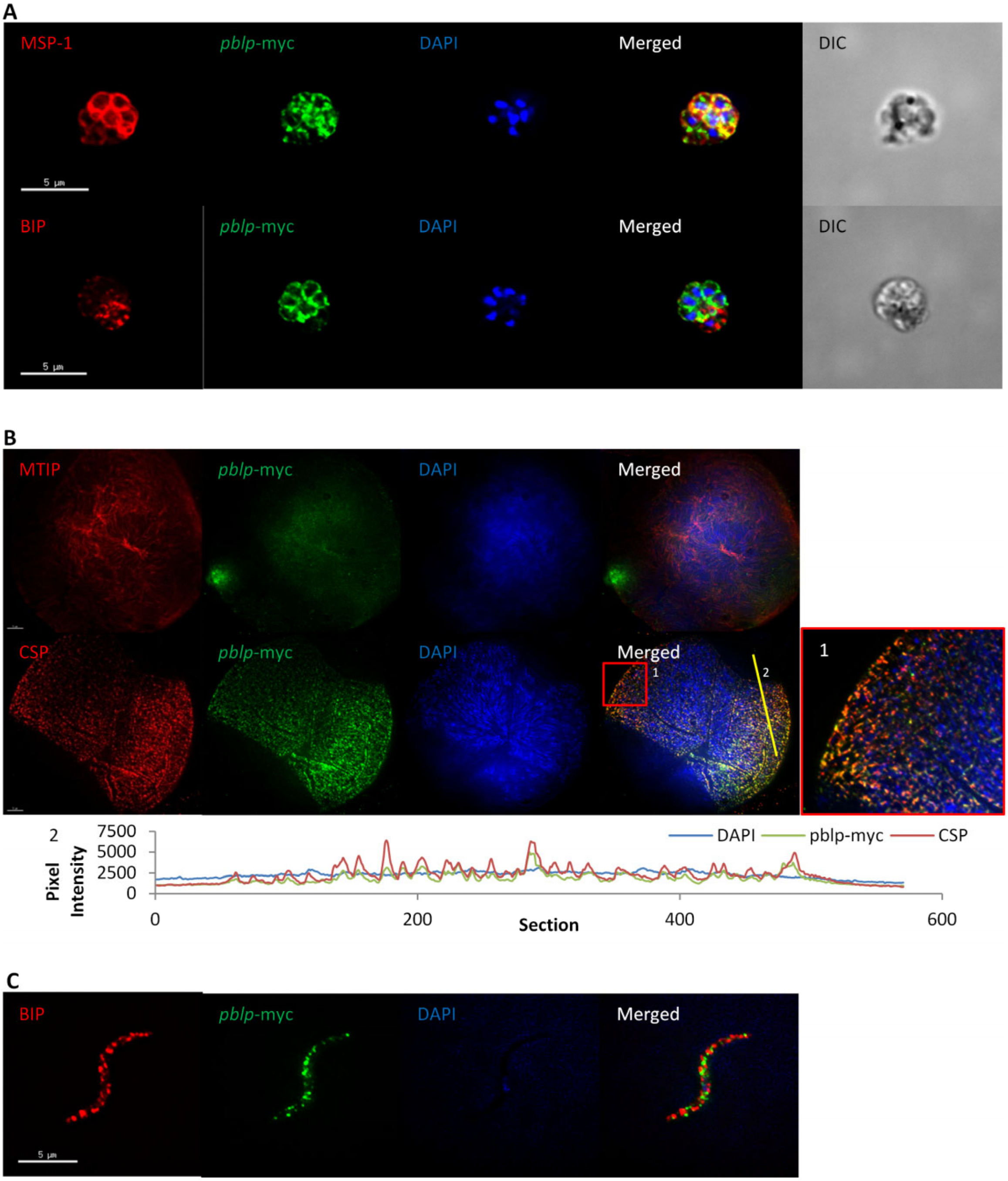

Fig. 2. Localization of *pblp*-myc tag parasites during the parasite life cycle.
A–F. (A) *pblp*-myc tag containing iRBCs, (B) mosquito midgut-derived oocysts, (C) salivary gland-derived sporozoites and liver sections from *pblp*-myc-tag-infected livers isolated at (D) 24, (E) 45 and (F) 52 hpi were stained to track PBLP localization using immunofluorescence microscopy. Enlarged sections of the merged fluorescence image had been outlined in red (*right*). Cross sections of the merged fluorescence image are indicated by yellow bars and the mean pixel intensity for each fluorophore along the 2D plane (left to right) was quantified using the softWoRx software (*below*). Cells were stained with a mouse monoclonal anti-PyBIP (ER marker, red), mouse monoclonal anti-PyMTIP (IMC marker, red), mouse monoclonal anti-PyHep17 (PVM marker, red), mouse monoclonal anti-PyCSP (PPM marker, red), mouse monoclonal anti-c-Myc (green), rabbit polyclonal anti-PfBIP (red), rabbit polyclonal anti-PyMSP-1 (PPM marker, red), a rabbit polyclonal anti-c-myc (green) and a goat polyclonal anti-c-myc antibody (green). DAPI (blue) was used to stain the nuclei of both parasites and host hepatocytes. Images of a representative sample are shown.

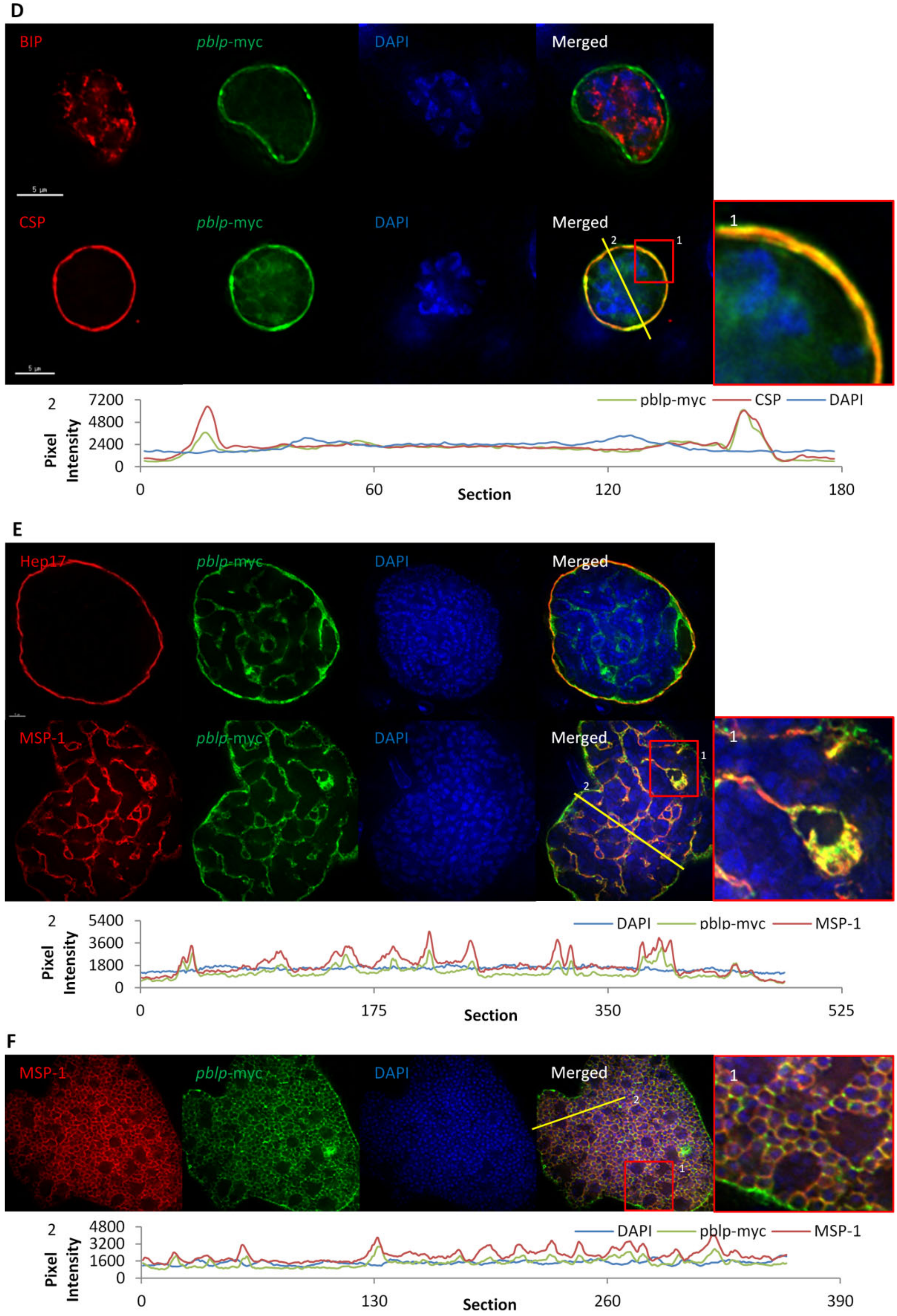

Fig. 2. *Continued.*

Δ*pblp* mixed-stage iRBCs and monitored the course of parasitemia until the mice were no longer patent (approximately 16 days) (Supporting Information Fig. S4). Interestingly, while Δ*pblp* parasites initially grew at the same rate as the WT parasites, there was a significant decrease in parasitemia levels throughout the course of the assay, indicating that the Δ*pblp* strains were unable to achieve the same level of growth as the WT parasites (Supporting Information Fig. S4). Similar results were observed with mice injected with 1×10^4 Δ*pblp* mixed-stage iRBCs (data not shown) or 1×10^6 Δ*pblp* schizont-containing iRBCs, the latter of which synchronized the initial BS inoculum and exacerbated the observed effect on BS growth (Fig. 3A). Despite the differences in parasitemia, all parasites were cleared from the mice at the same rate (Supporting Information Fig. S4 and Fig. 3A), implying that the effect on BS growth may be due to a developmental defect rather than the result of immune clearance. Thus, the Δ*pblp* strains appear unable to replicate at a similar rate as the WT during the intra-erythrocytic cycle (Fig. 3A).

Lower parasitemia could be explained by defects in invasion, delays in growth or a defect in merozoite formation, whereby fewer merozoites are produced by Δ*pblp* parasites. In order to better examine the defect in BS growth, we used IFA to characterize intra-erythrocytic parasite development (Fig. 3B–F). Interestingly, we observed no discernible difference in the formation of ring stages (data not shown) or trophozoites (data not shown), and while Δ*pblp* schizonts showed no defects in organelle segregation (Fig. 3C–E), PPM (Fig. 3B–F) or PVM formation (Fig. 3B and F); they formed smaller schizonts with visibly fewer merozoites when compared with WT parasites (Fig. 3B–F). In order to quantify the number of merozoites produced in iRBCs, schizonts were isolated as before, stained and analysed using a Delta Vision Spectris RT microscope. We took multiple optical sections for every schizont-containing iRBCs analysed (average of 30 schizont-containing iRBCs per condition) and calculated the number of merozoites observed in each section (4 sections/schizont) in order to account for changes in visible merozoites within different planes of the same schizont. We found that on average, both Δ*pblp* strains produced significantly fewer merozoites/iRBC as compared with the WT (Fig. 3G), indicating that PBLP has an important role in regulating the number of merozoites formed within schizonts.

Deletion of PBLP *affects sporozoite maturation and infectivity*

In order to determine if the Δ*pblp* strains were defective in sporozoite development or salivary gland infection, mosquito midguts and salivary glands were harvested from infected *A. stephensi* mosquitoes and analysed after 11 and 14 days post infectious blood meal (pIBM) respectively. Interestingly, while there were no observable differences in exflagellation, Δ*pblp* parasites produced approximately 30% fewer oocysts, resulting in significantly fewer oocyst-derived sporozoites as compared with the WT (Table 2). Although there was also a decrease in the number of salivary gland sporozoites of Δ*pblp* v1 and v2 as compared with the WT, it was roughly proportional to the reduction of oocyst-derived sporozoite numbers.

To ascertain what role PBLP might have in sporogony, WT and Δ*pblp* derived oocysts were isolated 11 days pIBM, stained and the number of budding sporozoites was quantified using a Delta Vision Spectris RT microscope with the same capture settings ($n = 27$–28). 4′,6-diamidino-2-phenylindole (DAPI) concentrations were used as a marker for the number of sporozoites produced within each developing oocyst (Fig. 4A) and quantified using the softWoRx program software (Fig. 4B). Since there was no significant difference in DAPI signal, both WT- and Δ*pblp*-derived oocysts produced similar sporozoite numbers (Fig. 4B), suggesting that the reason Δ*pblp* parasites produce fewer sporozoites is directly caused by the formation of fewer oocysts (Table 2). Given that PBLP co-localizes with CSP in developing oocysts (Fig. 2B), it is possible that although PBLP has no effect on the number of sporozoites produced within oocysts, it might affect other aspects of sporogony such as sporozoite maturation. To this end, sgSpz were isolated at 14 days pIBM and analysed by IFA using known organelle markers (Fig. 4C–E). Interestingly, Δ*pblp* sporozoites (v1 and v2) were visibly thinner than WT sporozoites with altered CSP staining although the inner membrane complex was unaffected when assessed by myosin A-tail interacting protein (MTIP) staining (Fig. 4C). Additionally, Δ*pblp* sporozoites displayed altered intracellular staining patterns for BIP (Fig. 4D) and TRAP (Fig. 4E), which implies that PBLP might have an additional role in sporozoite maturation.

We next assessed whether Δ*pblp* sporozoites exhibited decreased infectivity *in vivo*. Wild-type and Δ*pblp* sgSpz were isolated from infected mosquitoes and injected intravenously (IV) into BALB/cJ mice (1×10^3 or 1×10^4). The onset of BS parasitemia was then assessed every 12 h using Giemsa-stained thin blood smears. All of the mice that were infected with the WT sporozoites developed BS patency between 2 and 3 days post injection, depending on the dose (Table 3). However, while all of the mice that were infected with either Δ*pblp* strain became patent, there was a consistent 1 day delay in BS patency when compared with the same sporozoite dose of WT (Table 3). This phenotype could be partially explained by the observation that the Δ*pblp* strains (v1 and v2) produce fewer merozoites

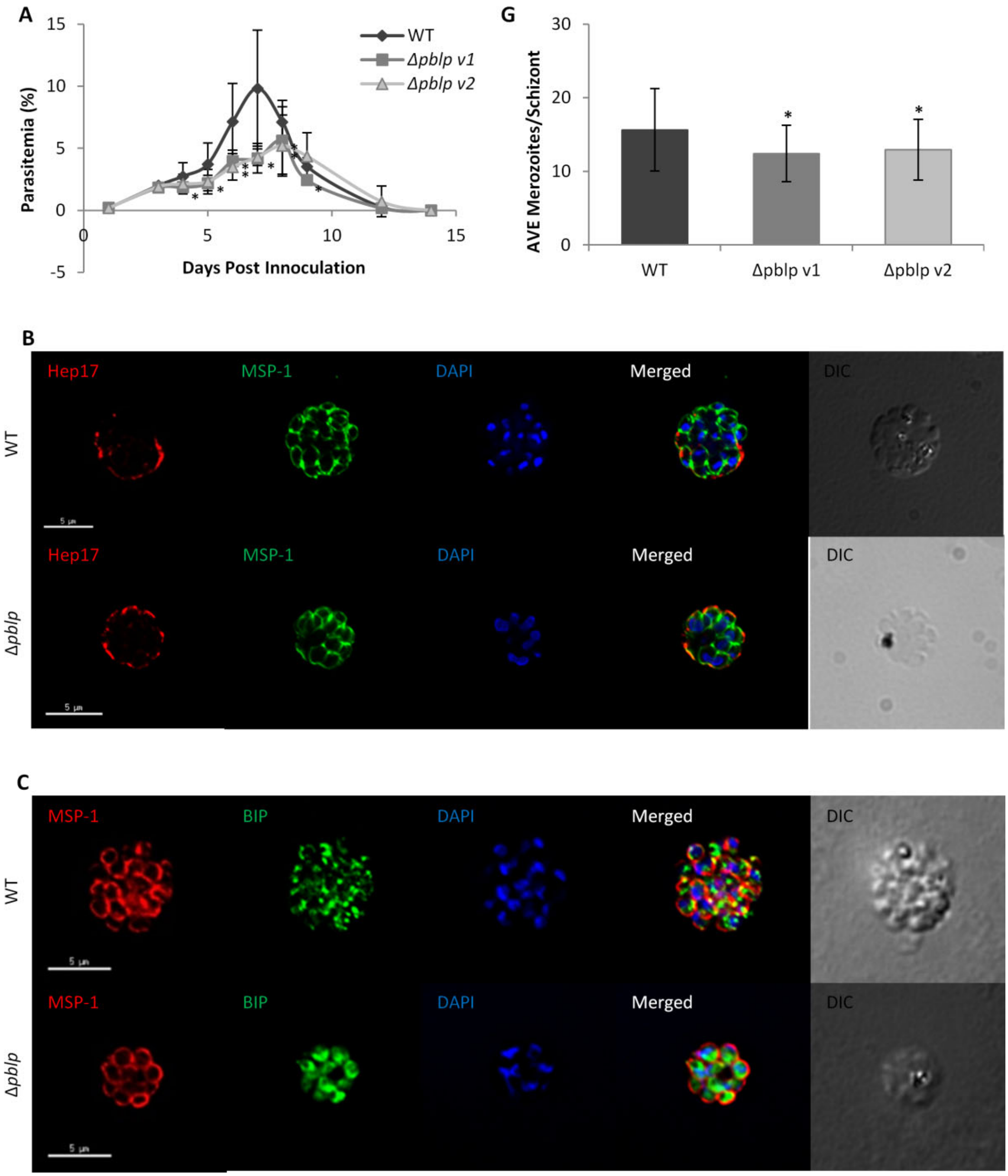

Fig. 3. Δ*pblp* parasites produce significantly fewer merozoites during intra-erythrocytic replication cycles, resulting in a diminished capacity to achieve WT replication levels *in vivo*.

A. BS growth curve using isolated schizonts. Mixed-stage blood samples were collected from WT ($n = 6$) or Δ*pblp* (v1 and v2, $n = 6$) infected SW and grown *in vitro* for 12 h to halt parasitic replication in the schizont phase. Schizont-containing erythrocytes were isolated using an Accudenz density cushion and 1×10^6 WT or Δ*pblp* (v1 and v2) schizonts were injected IV into BALB/cJ mice. Parasitemia in the blood was measured daily until all parasites were cleared. The data are a combination of two experimental replicates.

B–F. WT (*above*) Δ*pblp* (*below*) schizont-containing erythrocytes. Schizont-containing erythrocytes were isolated and purified from WT or Δ*pblp* (v1 and v2) infected mice and viewed by immunofluorescence microscopy. Schizonts were stained with a mouse monoclonal anti-PyMSP-1 (PPM marker, red), a mouse monoclonal anti-PyHep17 (PVM marker, red), a mouse monoclonal anti-PyACP (apicoplast marker, red), a mouse monoclonal anti-PyRon4 (rhoptry marker, red), a rabbit polyclonal anti-PfBIP (ER marker, green), a rabbit polyclonal anti-PyMSP-1 (green) and a rabbit polyclonal anti-PyMTIP antibody (IMC marker, green). Parasite DNA was stained with DAPI (blue).

G. Merozoites within WT ($n = 34$) or Δ*pblp* (v1 and v2, $n = 33$) infected erythrocytes were quantified from sequential slices (four values were averaged for each schizont quantified), which were generated using the Delta Vision Spectris RT microscope under 100× magnification. Images of a representative sample are shown. *P value ≤ 0.05.

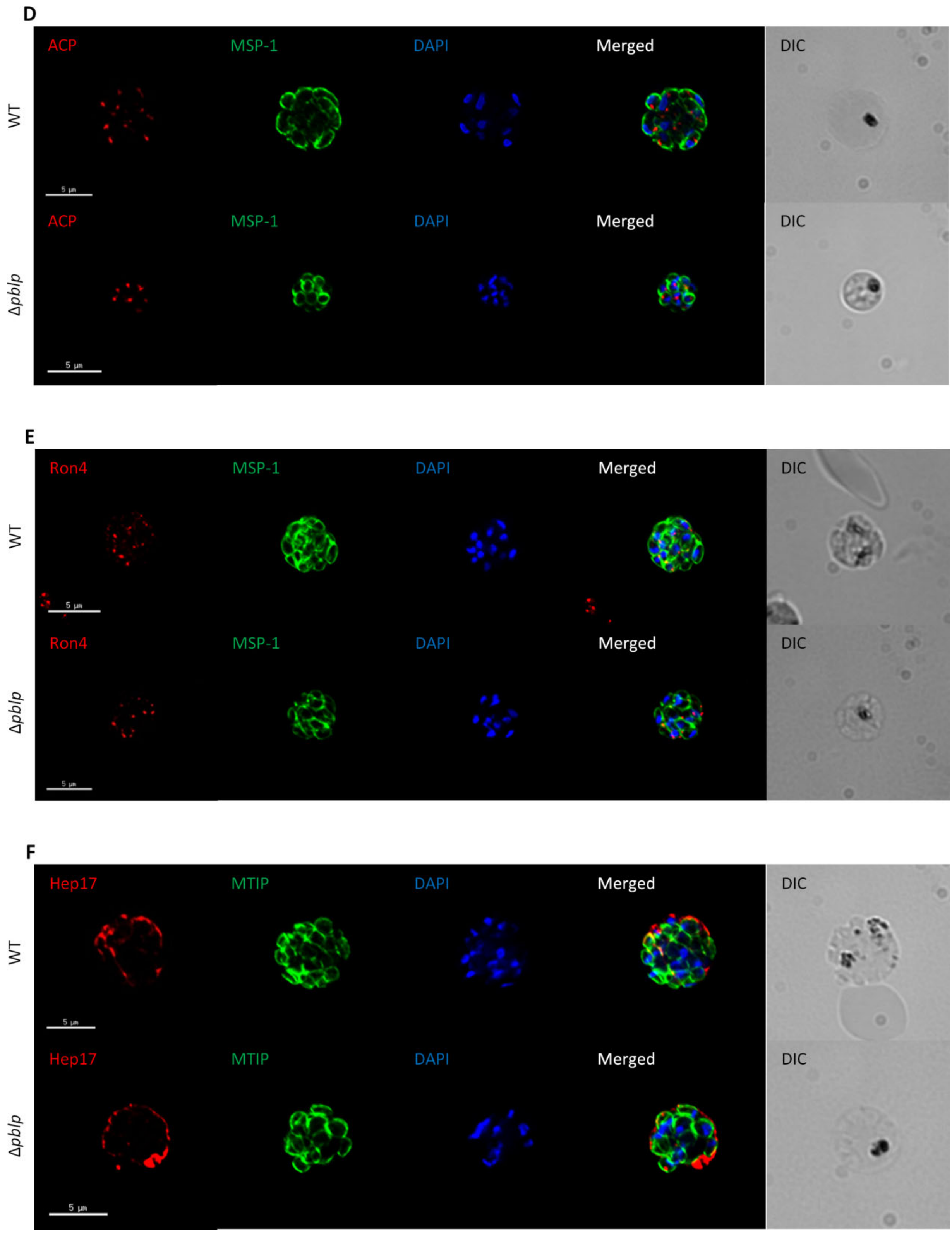

Fig. 3. *Continued.*

Table 2. Deletion of *pblp* has a significant impact on oocyst formation and sporozoite development in *Anopheles* mosquitoes.

Strain	Exflagellation[a,b]	Oocysts[a,c]	mgSpz[a,c]	sgSpz[a,d]
WT	5 ± 2	24 ± 12	72,200 ± 65,000	21,100 ± 16,000
Δ*pblp* v1	5 ± 2	15 ± 10*	28,300 ± 28,400*	10,800 ± 8,900*
Δ*pblp* v2	5 ± 1	17 ± 10*	23,900 ± 24,000*	8,400 ± 6,200*
pblp-myc #1	5 ± 1	21 ± 12	56,900 ± 41,400	22,200 ± 17,800
pblp-myc #2	5 ± 1	23 ± 16	69,000 ± 15,600	40,800 ± 34,800

**P* value ≤ 0.05.
a. Values are means ± standard deviations.
b. Exflagellation was quantified on day 3 post inoculation as relative number of events/field of view under 40× magnification (combination of >6 independent experiments with 2–3 mice per experiment).
c. Mosquito midgets were removed at 11 days pIBM and sporozoites were quantified (combination of at least six independent experiments with >10 mosquitoes per experiment).
d. Salivary glands were removed at 14 days pIBM and sporozoites were quantified (combination of at least six independent experiments with >30 mosquitoes per experiment).

during BS schizogony but decreased sporozoite infectivity and defects in LS development could also contribute to the delayed onset of patent parasitemia.

Δpblp sporozoites are defective in host cell traversal and invasion in vitro *and* in vivo

We next analysed whether defects in initial infection could contribute to the observed reduction in LS burden. An *in vitro* infection model was used to examine the rate of invasion and traversal of the Δ*pblp* strains and WT sporozoites by flow cytometry. Δ*pblp* and WT sgSpz were used to infect Hepa1-6 mouse hepatoma cells in the presence of dextran in order to assess cell wounding as a result of sporozoite traversal *in vitro*. After a 90 min incubation, the cells were fixed and stained with a fluorescent anti-CSP antibody in order to additionally identify infected cells. Interestingly, flow analysis determined that both Δ*pblp* strains showed a significant invasion and traversal defect as compared with WT parasites (Fig. 5A and B). Cell traversal allows mosquito-bite delivered sporozoites to cross the dermal cell barrier and enter the blood stream *in vivo* (Amino *et al*., 2008). Since Δ*pblp* sporozoites had a defect in traversal *in vitro*, we predicted that this would exacerbate the delay in onset of BS patency in mice infected by mosquito bite. To test this, WT or Δ*pblp*-infected *A. stephensi* mosquitoes were allowed to feed on BALB/cJ mice for 10 min. The onset of BS parasitemia was evaluated using Giemsa-stained thin blood smears and showed that if the Δ*pblp* infected mice became patent (approximately 89%), there was a 1–2 day delay when compared with mice infected IV with Δ*pblp* sporozoites (Table 3). To assess whether the Δ*pblp* sporozoite defect in traversal *in vitro* corresponded to a defect in motility, WT and Δ*pblp* sporozoites were isolated from infected salivary glands at day 14 pIBM and subjected to a CSP deposition assay (Fig. 5C and D). Δ*pblp* sporozoites were shown to be less motile than WT sporozoites, which partially explains the observation that Δ*pblp* parasites have a significant traversal defect (Table 3, Fig. 5B) although they are still capable of gliding and depositing CSP in concentric circles (Fig. 5C).

Δpblp parasites display a delay in LS development

Finally, we set out to determine whether Δ*pblp* parasites also exhibit a direct LS growth defect. We quantified the WT and Δ*pblp* parasite biomass in the liver by monitoring the abundance of parasite 18S rRNA from the livers of BALB/cJ-infected mice compared with total liver RNA (mouse GAPDH) at 45 hpi, which was then normalized to the relative abundance of the WT parasites. We found that the livers of mice infected with the Δ*pblp* strains showed an 80% (Δ*pblp* v1) or 95% (Δ*pblp* v2) reduction in parasite RNA as compared with those infected with the WT (Fig. 6A), which likely caused the observed delays in the onset of BS patency (Table 3).

Microscopic evaluation of infected livers revealed that the Δ*pblp* parasites were also significantly smaller that the WT parasites at 24 (data not shown) and 45 hpi (Fig. 6B). Furthermore, there was a 50% decrease in the number of Δ*pblp*-infected hepatocytes at 24 (data not shown) and 45 hpi when compared with the WT (Fig. 6C). To determine if Δ*pblp* parasites had a defect in late LS development, we assessed Δ*pblp* and WT liver sections using IFA, probing with markers that indicate LS developmental progression (Fig. 7). Interestingly, an analysis of multiple liver sections across several experiments showed that the Δ*pblp* parasites did not display the typical MSP-1 (Fig. 7A) or MSP-7 (data not shown) staining patterns observed in WT parasites at 45 hpi (Table 4). When the microscopic analysis was extended to earlier time points, it was determined that Δ*pblp* LS were different from WT LS at 24 (Fig. 7B) and 40 hpi (Fig. 7C). Additionally, characteristic MSP-1 (Fig. 7D) and MSP-7 (data not shown) staining patterns did not appear in Δ*pblp* LS until 52 hpi, which is when the majority of WT LS had already completely matured (Fig. 7D, Table 5). Indeed, Δ*pblp* LS parasites did not start

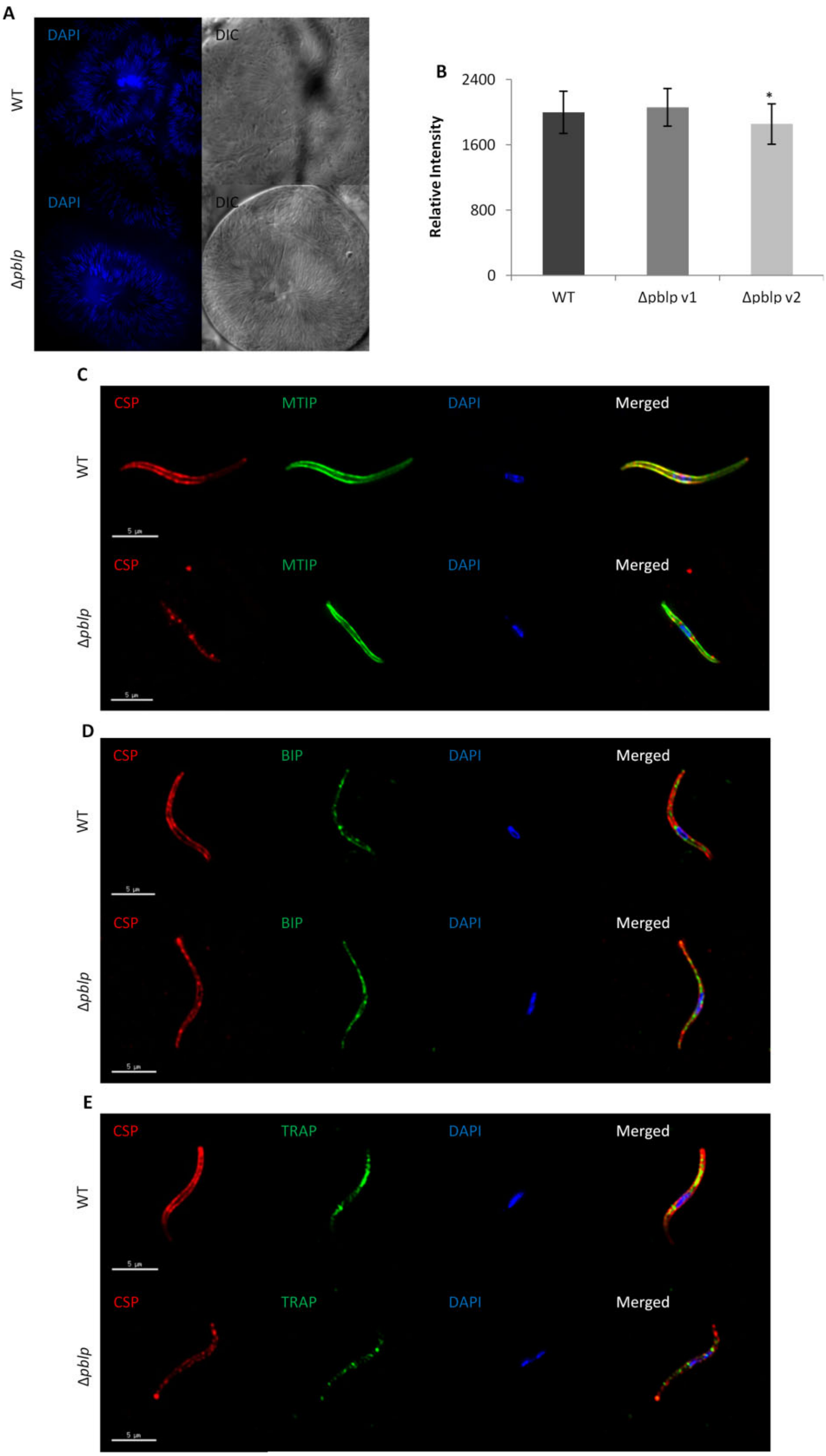

Fig. 4. Δ*pblp* parasites produce morphologically distinct sporozoites despite there being no difference in the total number of sporozoites produced within Δ*pblp*-derived oocysts.
A. WT (*above*) and Δ*pblp* (v1 and v2, *below*) derived oocysts were isolated from infected mosquitoes on day 11 pIBM and analysed using immunofluorescence microscopy. Parasite DNA was stained with DAPI (blue) and used as a marker for sporozoite number when all samples (WT and Δ*pblp*) were analysed using the same capture settings.
B. Sporozoite numbers were represented by DAPI signal intensity from deconvolved slices, which were generated using the Delta Vision Spectris RT microscope under 100× magnification. Quantification was done using the softWoRz software package.
C–E. Salivary gland-derived sporozoites were isolated from WT (*above*) and Δ*pblp* (v1 and v2, *below*) infected mosquitoes at day 14 pIBM and analysed using immunofluorescence microscopy. Sporozoites were stained with a mouse monoclonal anti-PyCSP (PPM marker, red), a rabbit polyclonal anti-PyMTIP (IMC marker, green), a rabbit polyclonal anti-PyBIP (ER marker, green) and a rabbit polyclonal anti-PyTRAP (microneme marker, green). Parasite DNA was stained with DAPI (blue). Images of a representative sample are shown. *P value ≤ 0.05.

Table 3. Δ*pblp* parasites (v1 and v2) show a delay in patency in BALB/cJ mice**.**

Genotype	Dose[a]	No. of mice	% Patent mice[b]	Mean days to patency[b]
WT	10^3	28	100	3.5
	10^4	27	100	2.5
	Mosquito bite	9	100	3
Δ*pblp* v1	10^3	9	100	4.5*
	10^4	6	100	3.5*
	Mosquito bite	9	89	5*
Δ*pblp* v2	10^3	8	100	4.5*
	10^4	9	100	3.5*
	Mosquito bite	9	890	5*
pblp-myc #1	10^3	8	100	3.5
	10^4	9	100	2.5
pblp-myc #2	10^3	6	100	3.5
	10^4	6	100	2.5

**P* value ≤ 0.05.
a. Number of sporozoites injected per mouse.
b. BS patency was monitored in mice every 12 h by thin smears.

producing exo-erythrocytic merozoites until 65 hpi (Fig. 7E), which indicates that PBLP is not only involved in establishing LS infections but that it also appears to modulate LS growth and development *in vivo*.

Discussion

In this study, we characterized a novel BEM46-like protein in *P. yoelii*, demonstrating that PBLP has a broad role in modulating the development of the parasitic infectious forms. All eukaryotic organisms carry a homologue of the *BEM46* gene (Mochizuki *et al*., 2005); however, only a few members of the α/β-hydrolase superfamily have been assigned functions. Members of the BEM46 family might modulate the function of morphogenic determinants, like the GTP–GDP exchange factor (GEF) or actin, on the cell surface. In *S. pombe*, the *BEM46* gene is a temperature-sensitive suppressor of the *S. cerevisiae bem1/bud5* double mutant (Valencik and Pringle, 1995). The exact function of BEM46 remains unknown in yeast; however, a functional analysis of BEM1 has suggested that BEM1 is a scaffold protein binding to BUD1, to the Cdc24p GEF for the Cdc42p Rho-like small G protein, to GTP-CDC42p, actin (Chenevert *et al*., 1992; Park *et al*., 1997; Cabib *et al*., 1998; Irazoqui *et al*., 2003) and to GDP–GTP exchange factors, such as BUD5 (Chant *et al*., 1991; Cabib *et al*., 1998), which are necessary for the positioning of a complex involved in bud formation. BUD5 is a GEF for BUD1 Ras-like small G protein and is necessary for bud site selection (Chant *et al*., 1991). It is believed that the *S. pombe* BEM46 protein combines the function of the yeast BEM1 and BUD5 proteins (Mercker *et al*., 2009), as does the *A. nidulans* homologue of BEM1, BemA, which plays a similar role in polarisome formation (Leeder and Tumer, 2008). Taken together, BEM46 proteins are implicated in signal transduction pathways that result in actin organization at the plasma membrane, which is why they appear to modulate cell surface morphology in multiple systems.

In this study, we show that PBLP localizes to the PPM in developing exo-erythrocytic schizonts, intra-erythrocytic schizonts, merozoites and oocysts. This localization is not unlike that of other BEM46 proteins and consistent with their ascribed role in determining cell morphology (Parmentier *et al*., 2000; Mercker *et al*., 2009) although the exact function of PBLP is still under investigation. In the weed *A. thaliana*, the BEM46 homologue is called wavy growth 2 (WAV2) and has been shown to negatively regulate stimulus-induced root bending through the inhibition of root tip rotation in response to environmental stimuli, localized to the plasma membrane and membranes of some organelles (Mochizuki *et al*., 2005). In *Drosophila*, the BEM46 homologue WAV2 plays a role in larval development (Parmentier *et al*., 2000; Giot *et al*., 2003), while in *N. crassa*, BEM46 is only required for hyphae development from germinating ascospores (Mercker *et al*., 2009). Given its localization at the plasma membrane, it is possible that PBLP plays a similar role in *Plasmodium*, modulating cellular differentiation of the invasive stages during sporogony and schizogony. However, PBLP does not appear to function in a cell-type specific manner since the Δ*pblp* parasites show defects in the development of all invasive stages. Since PBLP is conserved across *Plasmodium* spp., it is likely to have a shared function although it has not yet been characterized in additional *Plasmodium* species.

The BEM46-homologous gene *YNL320W* is a single-copy gene in *S. cerevisiae* but like most BEM46 proteins, it is not essential (Giaever *et al*., 2002). Interestingly, despite having a role in modulating the development of the invasive stages in *Plasmodium*, PBLP is not essential, implying a partially redundant or non-essential function throughout parasite development in the mosquito vector and mammalian host. We have identified a number of other putative BEM46 homologues in *P. yoelii*, although it is currently not known what role, if any, they may have in modulating cell surface morphology or whether they might compensate for PBLP in *P. yoelii* Δ*pblp* parasites. Since PBLP is membrane associated in LS and BS parasites, specifically co-localizing with MSP-1, it presents an excellent candidate to investigate the cell surface complexes that govern the development of invasive stages. Previous studies have shown that the MSP-1 complex plays an essential role in normal growth and survival in BS parasites, whereby MSPDBL1/2 are embedded for stabilization during host–parasite interactions (Lin *et al*., 2014). Previous studies show that the MSP-1 complex is shed into culture supernatant after successful invasion of the parasite (Blackman and Holder, 1992), and that known

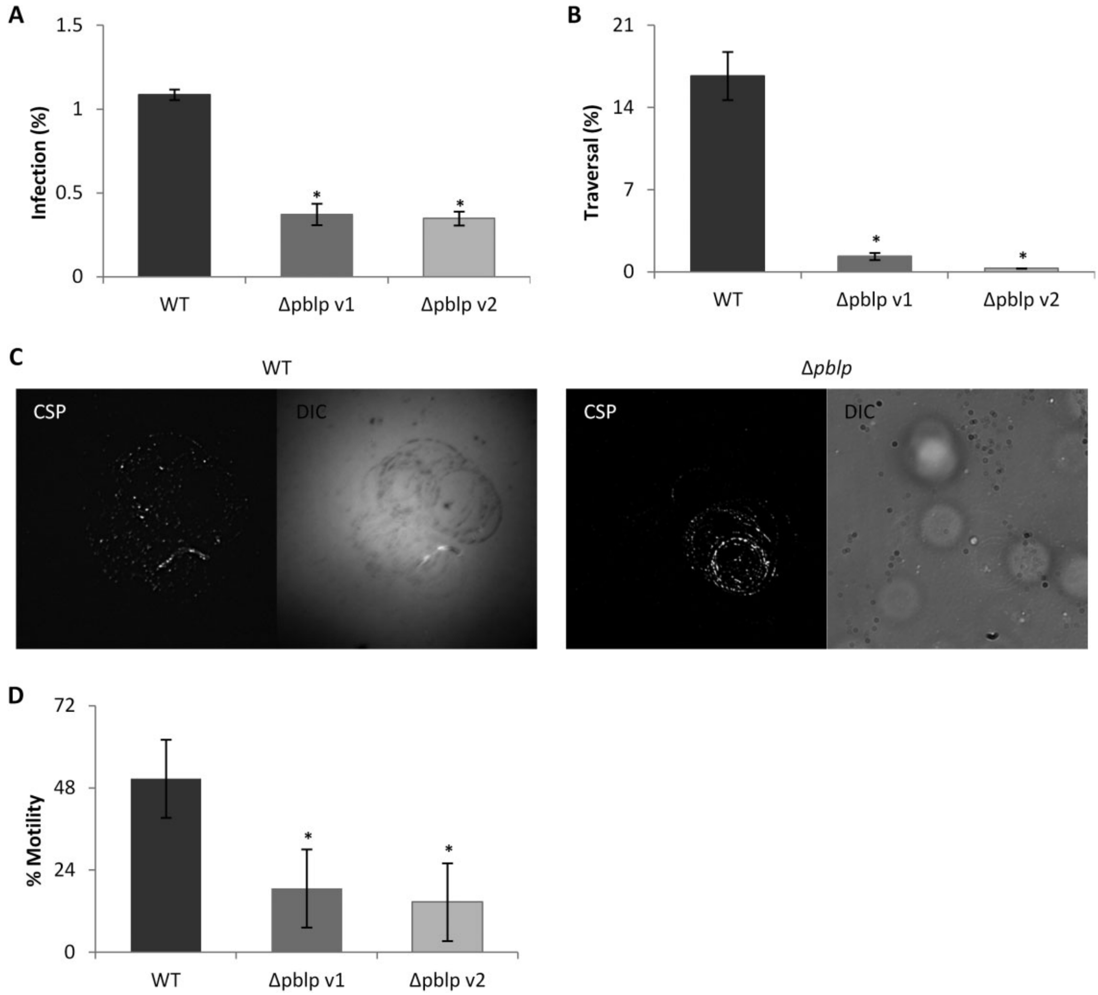

Fig. 5. Defects in hepatocyte infection. Hepa 1–6 cells were infected with 1×10^5 WT or Δ*pblp* (v1 and v2) salivary gland-derived sporozoites for 90 min with dextran conjugated to Alexa Fluor 488. We stained fixed cells using the monoclonal antibody against *Plasmodium yoelii* CSP, which was conjugated to AlexaFluor-647.
A and B. (A) Infected and (B) traversed hepatocytes were identified by FACS. WT (*left*) and Δ*pblp* (v1 and v2, *right*) salivary gland-derived sporozoites were subjected to a CSP deposition assay to assess relative motility on a glass surface using a monoclonal antibody against *P. yoelii* CSP, which was conjugated to AlexaFluor-594.
C. Motility was assessed from deconvolved slices, which were generated using the Delta Vision Spectris RT microscope under 100× magnification.
D. Quantification was carried out by counting the number of sporozoites that had completed at least one concentric circle in the time allowed (positive score) as it compared with the total number of sporozoites examined ($n \geq 75$). All experimental conditions were tested in biological triplicate. All data are representative of two independent experiments. Error bars depict standard deviation. Images of a representative sample are shown. $^*P$ value ≤ 0.05.

components of this complex include MSP-6 and MSP-7 (Pachebat *et al.*, 2001; Kauth *et al.*, 2006) although it is currently not clear whether there are multiple forms of the MSP-1 complex that consist of different proteins (Lin *et al.*, 2014). Since PBLP has been implicated in the development of the merozoite surface morphology in developing schizonts, it is possible that PBLP acts as a scaffolding protein and maintains the structural integrity of surface membrane protein complexes throughout the malaria life cycle. Alternatively, given the role of PBLP in the number of merozoites released from schizont-containing iRBCs, it is also possible that PBLP influences chromosome segregation during early LS schizogony since changes in DNA replication might explain why there are fewer nuclei produced in *Δpblp* BS parasites. The precise mechanism of action for how PBLP regulates the number of merozoites released from schizont-containing iRBCs remains to be elucidated.

In sporozoites, CSP is a GPI-anchored, highly conserved multifunctional protein that forms a dense coat on the parasite surface. It has been shown that deletion of CSP completely abrogates sporogony in oocysts and

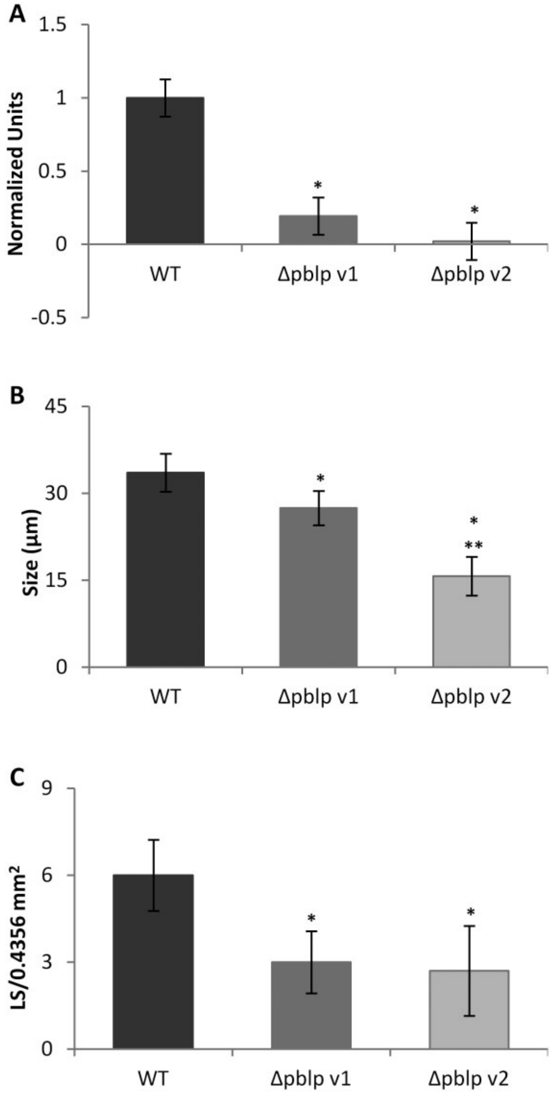

Fig. 6. Reduced parasite biomass in mice infected with Δ*pblp* parasites than in WT mice.
A. BALB/cJ mice were infected with 1×10^5 WT or Δ*pblp* parasites (v1 and v2) salivary gland-derived sporozoites. Livers were harvested at 45 hpi so that the relative amounts of parasite biomass could be determined by qPCR using primers directed against the parasite 18S rRNA. Experimental samples were first normalized to the mouse cellular GAPDH levels in each sample using specific primers in a parallel reaction and then the average transcript abundance for WT-infected livers was normalized to 1. Data reflect a representative sample from two repetitions ($n = 5$ mice per group).
B. Δ*pblp* LS parasites (v1 and v2) are smaller than WT at 45 hpi. LS diameters were measured from WT- or Δ*pblp*-infected livers ($n = 20$) using the ruler tool in the softWoRx software package. Three or four diameters were measured for each parasite and then averaged.
C. There are fewer Δ*pblp* LS parasites (v1 and v2) than WT. Livers from mice infected with 7.5×10^5 WT or Δ*pblp* salivary gland-derived sporozoites were analysed at 45 hpi. Quantification of the number of LS parasites per mm² of liver ($n = 11$). The data reflect a representative sample from two independent experiments. *P value ≤ 0.05.

reduced expression leads to abnormal sporozoite development, indicating a critical role for this protein in sporozoite budding (Ménard *et al*., 1997; Thathy *et al*., 2002; Ferguson *et al*., 2014), specifically affecting the later stages of sporogony rather than the initial stages of oocyst formation (Ferguson *et al*., 2014). We show here that PBLP co-localizes with CSP in oocysts and has an important role in regulating sporozoite development although the protein is localized to intracellular vesicles rather than the parasite surface in released sporozoites. It is not currently known whether the role of PBLP in oocyst sporozoite maturation is directly linked to the role of CSP in late-stage oocyst sporozoite development but the highly perturbed CSP localization in mature sporozoites strongly suggests a functional relationship between both proteins. Interestingly, MSP-1 did not exhibit similar perturbations in Δ*pblp* merozoites. Δ*pblp* sporozoites also suffered defects in gliding motility, cell traversal and cell invasion, which might well be attributable to their abnormal plasma membrane protein organization rather than to a direct role of PBLP in these processes.

Taken together, our data show that PBLP is a global modulator of the development of invasive stages in *Plasmodium.* Given its conservation within the BEM46 family of proteins, it is likely acting as a scaffold protein at the PPM during oocyst, LS and BS development although its precise mechanism of action remains unknown. Studies such as these provide invaluable insight into the molecular regulatory mechanisms that govern parasite invasive-stage morphogenesis.

Experimental procedures

Protein sequence analyses

For protein sequence conservation, protein sequences were aligned using the Clustal Omega web software (http://www.ebi.ac.uk/Tools/msa/clustalo/) from the European Bioinformatics Institute. For protein secondary structure prediction, protein sequences were analysed using the TOPO2 Transmembrane Protein Display software (http://www.sacs.ucsf.edu/cgi-bin/open-topo2.py/) from the Sequence Analysis and Consulting Service at University of California, San Francisco. For protein sequence similarity, protein sequences were analysed using a BLASTp (http://blast.ncbi.nlm.nih.gov/Blast.cgi) search from the National Center for Biotechnology Information or a BLASTn search on the PlasmoDB genomics resource from the EuPathDB Project Team (plasmodb.org/plasmo/). The PBLP nucleotide sequence, ORF organization and protein structure were derived using information from the PlasmoDB genomics resource from the EuPathDB Project Team.

Experimental animals, parasites and cell lines

Six- to eight-week-old female BALB/cJ (for *in vivo* infectivity and IFAs) or Swiss Webster (SW) (for parasite cycle maintenance)

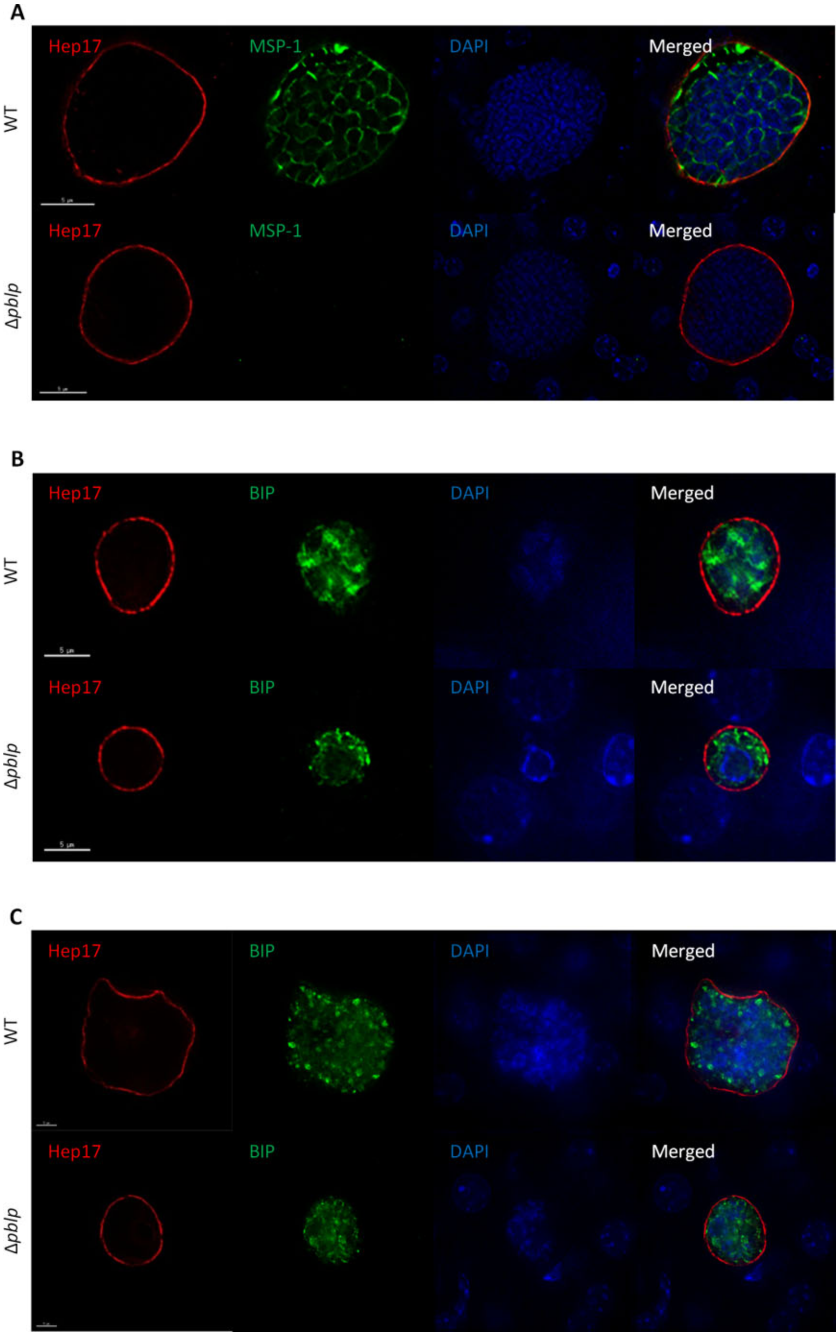

Fig. 7. Δ*pblp* parasites exhibit a developmental growth defect during LS development.
A–E. (A) Δ*pblp* parasites (v1 and v2) do not reach characteristic developmental milestones at the same rate as the WT parasites. Up to 7.5×10^5 WT (*above*) or Δ*pblp* (*below*) salivary gland-derived sporozoites were injected into BALB/cJ mice and livers were isolated at 45 hpi. Liver sections were stained with a mouse monoclonal antibody against *Plasmodium yoelii* Hep17 (red) to mark the PVM in infected hepatocytes while the PPM was visualized using a rabbit polyclonal antibody against *P. yoelii* MSP-1 (green). Parasite DNA is stained with DAPI (blue). LS development for WT (*above*) and Δ*pblp* (*below*) parasites (v1 and v2) in livers was monitored using a mouse monoclonal anti PyHep17 (red or green), a rabbit polyclonal anti-PfBIP (ER marker, green) or a rabbit polyclonal anti-PyMSP-1 antibody (green or red). Parasite DNA is stained with DAPI (blue). Livers were isolated from BALB/cJ mice infected with 7.5×10^5 WT or Δ*pblp* salivary gland-derived sporozoites at (B) 24, (C) 40, (D) 52 or (E) 65 hpi. Images of a representative sample are shown.

mice were purchased from the Jackson Laboratory or Harlan. Animal handling was conducted according to Institutional Animal Care and Use Committee-approved protocols. Wild-type *P. yoelii* 17XNL (nonlethal strain) clone 1.1 (WHO, 2010) and *P. yoelii* 17XNL transgenic parasites were cycled between SW mice and *A. stephensi* mosquitoes. We used infected SW mice to feed female *A. stephensi* mosquitoes after gametocyte exflagellation was observed. Data reflect the average of at least six independent experiments. Infected mosquitoes were maintained on sugar water at 24°C and 70% humidity and sporozoites were extracted from infected mosquitoes on day 11 (from midguts) and day 14 (from salivary glands) post blood meal infection as described before (Labaied *et al.*, 2007; Tarun *et al.*, 2007). Hepa 1–6 cells (for *in vitro* infection studies) were a gift from Ana Rodriguez (NYU). Cells were maintained in Dulbecco's modified eagle's medium complete media (Cellgro), supplemented with 10% Fetal Bovine Serum (FBS; Sigma-Aldrich), 100 IU ml^{-1} of penicillin (Cellgro), 100 mg ml^{-1} of streptomycin (Cellgro) and 5 mg ml^{-1} of gentamicin (BioWhittaker).

Generation of P. yoelii *transgenic parasites*

Gene targeting constructs for transgenic parasite production were designed as previously described (Mikolajczak *et al.*, 2008;

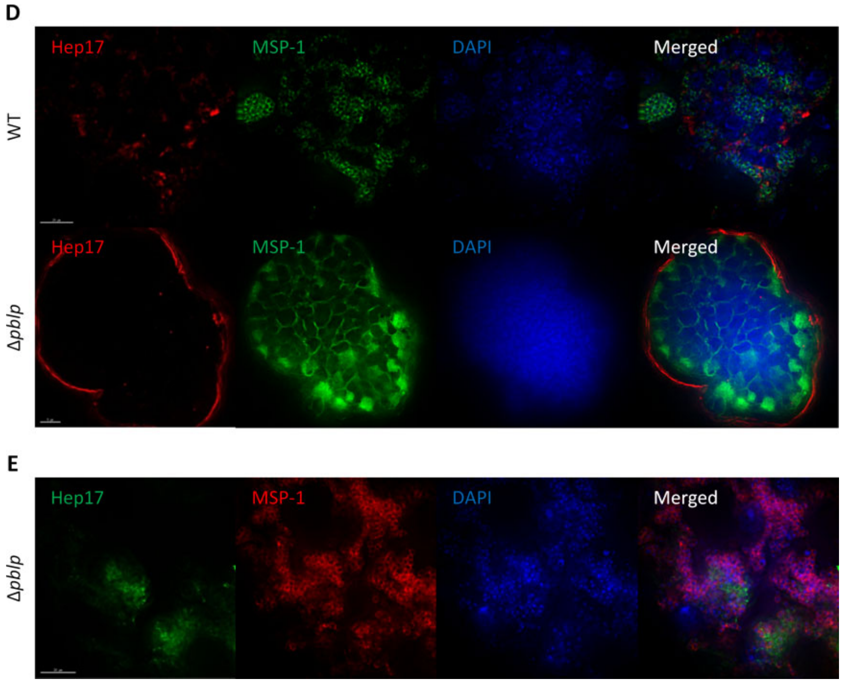

Fig. 7. *Continued.*

Lindner *et al.*, 2013a) with some modifications. Briefly, regions flanking the PBLP ORF (for Δ*pblp* constructs) or the last two exons of the ORF (for *pblp*-myc tag constructs) were amplified from WT genomic DNA using overlap extension-PCR (SOE-PCR) (Lindner *et al.*, 2013a). Resulting products were digested with KpnI/NotI (Δ*pblp*) or KpnI/SpeI (*pblp*-myc tag), gel isolated (Macherey-Nagel) and ligated into a modified pDEF vector that was designed for genetic disruptions or for gene modifications by locus replacement via double-crossover recombination. Prior to transfection, plasmids were linearized with ApaI (designed to separate the two halves of the targeting sequences), gel isolated and dissolved in water. The pDEF vector that was used to delete the PBLP ORF was designed to express green fluorescent protein under the control of the *P. berghei* EF1a promoter whereas the tagging pDEF vector fused a 4X myc tag to the C-terminus of the PBLP ORF. Transfection of WT parasites was conducted using an Amaxa Nucleofector device (Lonza) according to manufacturer's instructions with some modifications (Miller *et al.*, 2012; Lindner *et al.*, 2013a) and the resulting parasites were used to infect SW mice IV by tail-vein injection. Mice were subjected to drug selection with 7 $\mu g\ ml^{-1}$ of pyrimethamine (Sigma-Aldrich) and the presence of transgenic parasites was assessed by genotyping PCR. At least two independent clones of each transgenic parasite were isolated by limiting dilution infection of female SW mice (Janse *et al.*, 2006). Primer sequences are available upon request.

Table 4. The LS defect observed in Δ*pblp* parasites (v1 and v2) is caused in part by a LS developmental delay.

0.4356 mm^2	MSP-1 (+) (%)	MSP-1 (–) (%)
WT	89.3	10.7
Δ*pblp* v1	0*	100*
Δ*pblp* v2	0*	100*

**P* value ≤ 0.05.

Table 5. Δ*pblp* parasites (v1 and v2) do not mature at the same rate as WT parasites *in vivo*.

0.4356 mm^2	Immature schizont (%)	Mature schizont (%)
WT	27.3	72.7
Δ*pblp* v1	92.3*	7.7*
Δ*pblp* v2	92*	8*

**P* value ≤ 0.05.

RT-PCR and qPCR

Total RNA was extracted using TRIzol reagent (Invitrogen) from WT-infected mosquitoes salivary gland sporozoites (2×10^6), mixed BS parasites [1×10^7 red blood cells (RBCs) were isolated from an infected mouse by cardiac puncture] or infected livers (small liver lobes were vivisected from infected BALB/c mice at various times post infection with salivary gland sporozoites) and then treated with Turbo DNase (Ambion). For RT-PCR, cDNA synthesis was performed using a QuantiTect reverse transcription kit according to the manufacturer's instructions (Qiagen). Specific primers targeting the WT 18S or PBLP ORF were then used in a standard PCR reaction (95°C for 30 s for DNA denaturation, 52°C for 30 s for primer annealing and 62°C for 4 min for DNA strand extension; 35 amplification cycles). For semiquantitative PCR (qPCR), a standard curve was generated using 1:4 serial dilutions of a reference cDNA sample for PCR amplification of all target PCR products. Specific primers targeting the WT 18S were then used to compare expression levels (done in triplicate) across samples using an Applied Biosystems 7300 Real Time PCR System according to manufacturer's instructions with some modifications (95°C for 15 s for DNA denaturation, 60°C for 1 min for primer annealing and DNA strand extension; 40 amplification cycles). For the purposes of determining relative parasite biomass, the experimental samples were first normalized to the mouse cellular GAPDH levels in each sample using specific primers in a parallel reaction and then the average transcript abundance for WT-infected livers was normalized to 1. Primer sequences are available upon request.

Measurement of sporozoite development

Mosquitoes infected with WT or transgenic parasites were dissected at 11 and 14 days post blood meal infection to isolate midguts and salivary glands by standard methods. Oocyst burden and evidence of midgut sporozoite development was assessed by light microscopy at 40× magnification and average oocyst burden was determined by counting ($n > 10$) at 10× magnification. Average midgut and salivary gland sporozoite numbers per mosquito were determined by counting appropriately diluted samples ($n \geq 20$ mosquitoes) on a haemocytometer at 40× magnification. Data reflect the average of at least six independent experiments.

Detection of BS patency

Sporozoites were isolated from WT or transgenic-infected mosquitoes by microdissection from mosquito salivary glands at 14 days post blood meal infection as previously described (Aly *et al.*, 2011). BALB/cJ mice were injected IV (tail vein) with either 1000 or 10 000 salivary gland sporozoites or by the bite of 15 infected *A. stephensi* mosquitoes, as previously described (Sack *et al.*, 2014). Briefly, animals were anaesthetized with a mixture of ketamine and xylazine and placed on a feeding cage containing 15 infected mosquitoes. Mosquitoes were allowed to feed on the mice for 10 min but were lifted every minute and rotated among feeding cages every 2 min to ensure that all mice were equally exposed to infected mosquito bites. A sample of at least 20 mosquitoes from each feed was dissected to ensure sufficient mosquito infection. The time to BS patency (defined as ≥ 1 infected RBCs/10 000 RBCs) was scored microscopically by Giemsa-stained thin blood smears. A 1 day delay in the time to BS patency correlates with a 90% reduction in sporozoite infectivity (Gantt *et al.*, 1998). Three biological replicates were measured for each condition.

BS parasite growth curves

For mixed-stage growth curves, blood from SW mice infected with WT or Δ*pblp* parasites was harvested and diluted with RPMI 1640 (Corning). For schizont growth curves, blood from SW mice infected with WT or Δ*pblp* parasites was harvested and cultured in RPMI 1640 with 20% FBS (Sigma-Aldrich) and 50 μg ml^{-1} of gentamicin (BioWhittaker) for 12 h. After incubation, all infected RBCs (schizont stage) were isolated by centrifugation at 200 × g for 25 min using a 60% Accudenz density cushion. Mixed-stage blood parasites or isolated schizonts were diluted with RPMI 1640 and 1×10^6 parasites (WT or Δ*pblp*) were injected IV (tail vein) into each experimental BALB/cJ mouse. Parasitemia was tracked by analysing Giemsa-stained thin blood smears daily until clearance. Three biological replicates were measured for each condition.

Immunofluorescence assays

Oocysts. Mosquito midguts were isolated on day 11 pIBM and fixed in 4% formalin (Sigma-Aldrich) for 30 min at room temperature (RT). Midguts were washed twice with phosphate-buffered saline (PBS) before being permeabilized in 0.1% Triton X-100 in PBS for 30 min at RT. Permeabilized midguts were resuspended in 10% bovine serum albumin (BSA) in PBS. Blocking was carried out in an orbital shaker with constant motion for 2 h at RT.

Sporozoites. Midgut and salivary gland sporozoites were isolated on day 11 or 14 pIBM (respectively) and fixed in 4% formalin for 10 min at RT. Sporozoites were washed twice with PBS before being permeabilized in 0.1% Triton X-100 in PBS for 10 min at RT. Permeabilized sporozoites were resuspended in 3% BSA in PBS and then applied to a polylysine-treated slide, which was housed in a wet chamber at 4°C overnight.

Mixed-stage blood/schizonts. Infected RBCs or isolated schizonts (WT and transgenic) were washed in PBS before being fixed in 4% paraformaldehyde (PFA; Sigma-Aldrich) with 0.75% glutaraldehyde (Sigma-Aldrich) for 30 min with end-over-end rotation at RT. Samples were washed twice in PBS, fixed in 0.1% Triton X-100 in PBS for 10 min and finally resuspended in 3% BSA in PBS. Blocking was carried out with end-over-end rotation for 2 h at RT.

Liver sections. To visualize *in vivo* development of WT or transgenic parasites in livers, BALB/c mice were injected IV (tail vein) with $7.5 \times 10^5 - 2 \times 10^6$ sporozoites. Livers from the infected mice were harvested by vivisection, washed extensively with PBS and fixed in 4% PFA at several time points post infection (24, 40, 45, 52 and 65 h). Fifty micrometer sections were cut from fixed livers using a Vibratome apparatus (Ted Pella Inc.). IFAs were performed as previously described (Vaughan *et al.*, 2009). All samples were stained at RT (1 h) or 4°C (overnight) with the following appropriately diluted primary antibodies: mouse monoclonal anti-PyCSP (clone 2F6), mouse monoclonal anti-PyHep17 (Charoenvit *et al.*, 1995), mouse monoclonal anti-PyMSP-1 (clone 83a), mouse monoclonal anti-PyBIP, mouse monoclonal anti-PyACP, mouse monoclonal anti-PyRon4 (clone 48F8), mouse monoclonal anti-myc (Roche, #11667149001), rabbit polyclonal anti-PfBIP, rabbit polyclonal anti-PyTRAP, rabbit polyclonal anti-PyMSP-1, rabbit polyclonal anti-PyMTIP, rabbit anti-c-myc (Santa Cruz, SC-789) and goat anti-c-myc (Abcam, ab9132). Alexa Fluor-conjugated secondary antibodies specific to mouse, rabbit or goat IgG (Alexa Fluor 488, 594; Invitrogen) and DAPI. Samples were mounted onto glass slides using VectaShield (Vector Laboratories). Fluorescence and differential interference contrast (DIC) images were acquired using a Delta Vision Spectris RT microscope (Applied Precision) using a 60× or 100× oil objective and deconvolved and quantified using the softWoRx software package. All data show representative images from two to three independent experiments.

In vitro *invasion and traversal assay*

Hepa 1–6 cells were plated in 24-well plates (VWR) at a density of 3×10^5 cells/well and incubated overnight at 37°C with 5% CO_2. On the second day, salivary gland sporozoites were dissected from infected mosquitoes (WT or Δ*pblp*) and incubated with 20% FBS in RPMI 1640 and 250 μg ml^{-1} of dextran conjugated to Alexa Fluor 488 (Invitrogen) for 30 min at RT (assess cell permeabilization due to sporozoite traversal). Next, 1×10^5 sporozoites were added to each well, with a subsequent spin at 1500 r.p.m. for 5 min at RT. Cells were incubated at 37°C with 5% CO_2 for 90 min before being trypsinized and then fixed with Perm/Fix buffer (BD Biosciences). Cells were blocked in Perm/Wash buffer (BD Biosciences) supplemented with 2% BSA. A mouse monoclonal anti-CSP antibody conjugated to Alexa Fluor 647 was added for 45 min at RT. Cells were washed twice in PBS with 5 mM of ethylenediaminetetraacetic acid (Sigma-Aldrich) and then filtered using BD Falcon FACS tubes. Parasitized and traversed hepatocytes were identified by FACS using a BD LSRII and flow-cytometry analysis was performed using FlowJo software (TreeStar). All data are representative of three independent experiments.

CSP deposition assay

Fifty thousand sporozoites were seeded on uncoated full length coverslips (VWR), which had been pre-coated with mouse monoclonal anti-PyCSP (clone 2F6) diluted in PBS and left in a humid chamber at 4°C overnight. Sporozoites were dissected in RPMI-1640 with 20% FBS and incubated for 1 h at 37°C for settlement and gliding. After fixation with 4% formalin, for 10 min at RT, sporozoites were washed once with PBS and blocking was carried out in 3% BSA in PBS for 1 h at RT in a humid chamber. Sporozoites and trails were detected by incubation with a mouse monoclonal anti-PyCSP antibody IgG conjugated to Alexa Fluor 594 for 1 h at RT. Coverslips were washed twice in PBS and mounted using VectaShield medium to glass slides. Fluorescence and DIC images were acquired using a Delta Vision Spectris RT microscope using a 100× oil objective and deconvolved and quantified using the softWoRx software package. Quantification was performed by direct microscopic counting of three independent experiments.

Statistical analysis

Statistical analyses were performed in *Mstat* on two or more independent experiments (Wilcoxon rank sum test), as noted in the figure legends or text. Statistical significance was defined as $^*P < 0.05$.

Acknowledgements

We are grateful to Sebastian Mikolajczak and Ashley Vaughan for technical and scientific advice throughout the project. We appreciate Alexis Kaushansky for editing the manuscript. This work was supported by NIH/NIAID grant 5R01AI053709-11 (to SK).

References

Aly, A.S.I., and Matuschewski, K. (2005) A malarial cysteine protease is necessary for *Plasmodium* sporozoite egress from oocysts. *J Exp Med* **202:** 225–230.

Aly, A.S.I., Lindner, S.E., MacKellar, D.C., Peng, X., and Kappe, S.H.I. (2011) SAP1 is a critical post-transcriptional regulator of infectivity in malaria parasite sporozoite stages. *Mol Microbiol* **79:** 929–939.

Amino, R., Thiberge, S., Martin, B., Celli, S., Shorte, S., Frischknecht, F., and Ménard, R. (2006) Quantitative imaging of *Plasmodium* transmission from mosquito to mammal. *Nat Med* **12:** 220–224.

Amino, R., Giovannini, D., Thiberge, S., Gueirard, P., Boisson, B., Dubremetz, J.F., *et al.* (2008) Host cell traversal is important for progression of the malaria parasite through the dermis to the liver. *Cell Host Microbe* **3:** 88–96.

Arnot, D.E., and Gull, K. (1998) The *Plasmodium* cell-cycle: facts and questions. *Ann Trop Med Parasitol* **92:** 361–365.

Bannister, L.H., Hopkins, J.M., Fowler, R.E., Krishna, S., and Mitchell, G.H. (2000) A brief illustrated guide to the ultrastructure of *Plasmodium falciparum* asexual blood stages. *Parasitol Today* **16:** 427–433.

Blackman, M.J., and Holder, A.A. (1992) Secondary processing of the *Plasmodium falciparum* merozoite surface protein-1 (MSP1) by a calcium-dependent membrane-bound serine protease: shedding of MSP133 as a noncovalently associated complex with other fragments of the MSP1. *Mol Biochem Parasitol* **50:** 307–315.

Bray, R.S., and Garnham, P.C. (1982) The life-cycle of primate malaria parasites. *Br Med Bull* **38:** 117–122.

Cabib, E., Drgonova, J., and Drgon, T. (1998) Role of small G proteins in yeast cell polarization and wall biosynthesis. *Annu Rev Biochem* **67:** 307–333.

Chant, J., Corrado, K., Pringle, J.R., and Herskowitz, I. (1991) Yeast *BUD5*, encoding a putative GDP-GTP exchange factor, is necessary for bud site selection and interacts with bud formation gene BEM1. *Cell* **65:** 1213–1224.

Charoenvit, Y., Mellouk, S., Sedegah, M., Toyoshima, T., Leef, M.F., De La Vega, P., *et al.* (1995) *Plasmodium yoelii:* 17-kDa hepatic and erythrocytic stage protein is the target of an inhibitory monoclonal antibody. *Exp Parasitol* **80:** 419–429.

Chenevert, J., Corrado, K., Bender, A., Pringle, J.R., and Herskowitz, I. (1992) A yeast gene (BEM1) necessary for cell polarization whose product contains two SH3 domains. *Nature* **356:** 77–79.

Cowman, A.F., and Crabb, B.S. (2006) Invasion of red blood cells by malaria parasites. *Cell* **124:** 755–766.

Ferguson, D.J., Balaban, A.E., Patzewitz, E.M., Wall, R.J., Hopp, C.S., Poulin, B., *et al.* (2014) The repeat region of the circumsporozoite protein is critical for sporozoite formation and maturation in *Plasmodium*. *PLoS ONE* **9:** e113923.

Gantt, S.M., Myung, J.M., Briones, M.R.S., Li, W.D., Corey, E.J., Omura, S., *et al.* (1998) Proteasome inhibitors block development of *Plasmodium spp*. *Antimicrob Agents Chemother* **42:** 2731–2738.

Giaever, G., Chu, A.M., Ni, L., Connelly, C., Riles, L., Veronneau, S., *et al.* (2002) Functional profiling of the *Saccharomyces cerevisiae* genome. *Nature* **418:** 387–391.

Giot, L., Bader, J.S., Brouwer, C., Chaudhuri, A., Kuang, B., Li, Y., *et al.* (2003) A protein interaction map of *Drosophila melanogaster*. *Science* **302:** 1727–1736.

Golenda, C.F., Starkweather, W.H., and Wirtz, R.A. (1990) The distribution of circumsporozoite protein (CS) in *Anopheles stephensi* mosquitoes infected with *Plasmodium falciparum* malaria. *J Histochem Cytochem* **38:** 475–481.

Holmquist, M. (2000) Alpha/Beta-hydrolase fold enzymes: structures, functions and mechanisms. *Curr Protein Pept Sci* **1:** 209–235.

Irazoqui, J.E., Gladfelter, A.S., and Lew, D.J. (2003) Scaffold mediated symmetry breaking by Cdc42p. *Nat Cell Biol* **5:** 1062–1070.

Janse, C.J., Franke-Fayard, B., Mair, G.R., Ramesar, J., Thiel, C., Engelmann, S., *et al.* (2006) High efficiency transfection of *Plasmodium berghei* facilitates novel selection procedures. *Mol Biochem Parasitol* **145:** 60–70.

Jin, Y., Kebaier, C., and Vanderberg, J. (2007) Direct microscopic quantification of dynamics of *Plasmodium berghei* sporozoite transmission from mosquitoes to mice. *Infect Immun* **75:** 5532–5539.

Kauth, C.W., Woehlbier, U., Kern, M., Mekonnen, Z., Lutz, R., Mücke, N., *et al.* (2006) Interactions between merozoite surface proteins 1, 6, and 7 of the malaria parasite *Plasmodium falciparum*. *J Biol Chem* **281:** 31517–31527.

Labaied, M., Camargo, N., and Kappe, S.H.I. (2007) Depletion of the *Plasmodium berghei* thrombospondin-related sporozoite protein reveals a role in host cell entry by sporozoites. *Mol Biochem Parasitol* **153:** 158–166.

Leeder, A.C., and Tumer, G. (2008) Characterisation of *Aspergillus nidulans* polarisome component BemA. *Fungal Genet Biol* **45:** 897–911.

Lin, C.S., Uboldi, A.D., Marapana, D., Czabotar, P.E., Epp, C., Bujard, H., *et al.* (2014) The merozoite surface protein 1 complex is a platform for binding to human erythrocytes by *Plasmodium falciparum*. *J Biol Chem* **289:** 25655–25669.

Lindner, S.E., Mikolajczak, S.A., Vaughan, A.M., Moon, W., Joyce, B.R., Sullivan, W.J., Jr, and Kappe, S.H.I. (2013a) Perturbations of *Plasmodium* Puf2 expression and RNA-seq of Puf2-deficient sporozoites reveal a critical role in maintaining RNA homeostasis and parasite transmissibility. *Cell Microbiol* **15:** 1266–1283.

Lindner, S.E., Swearingen, K.E., Harupa, A., Vaughan, A.M., Sinnis, P., Moritz, R.L., and Kappe, S.H. (2013b) Total and putative surface proteomics of malaria parasite salivary gland sporozoites. *Mol Cell Proteomics* **12:** 1127–1143.

Madden, K., and Snyder, M. (1998) Cell polarity and morphogenesis in budding yeast. *Annu Rev Microbiol* **52:** 687–744.

Margos, G., Bannister, L.H., Dluzewski, A.R., Hopkins, J., Williams, I.T., and Mitchell, G.H. (2004) Correlation of structural development and differential expression of invasion-related molecules in schizonts of *Plasmodium falciparum*. *Parasitology* **129:** 273–287.

Ménard, R., Sultan, A.A., Cortes, C., Altszuler, R., van Dijk, M.R., Janse, C.J., *et al.* (1997) Circumsporozoite protein is required for development of malaria sporozoites in mosquitoes. *Nature* **385:** 336–340.

Meis, J.F., Verhave, J.P., Jap, P.H., and Meuwissen, J.H. (1983) An ultrastructural study on the role of Kupffer cells in the process of infection by *Plasmodium berghei* sporozoites in rats. *Parasitology* **86:** 231–242.

Meis, J.F., Ponnudurai, T., Mons, B., van Belkum, A., van Eerd, P.M., Druilhe, P., and Schellekens, H. (1990) *Plasmodium falciparum:* studies on mature exoerythrocytic forms in the liver of the chimpanzee, *Pan troglodytes*. *Exp Parasitol* **70:** 1–11.

Mercker, M., Kollath-Leiss, K., Allgaier, S., Weiland, N., and Kempken, F. (2009) The BEM46-like protein appears to be essential for hyphal development upon ascospore germination in *Neurospora crassa* and is targeted to the endoplasmic reticulum. *Curr Genet* **55:** 151–161.

Mikolajczak, S.A., Aly, A.S.I., Dumpit, R.F., Vaughan, A.M., and Kappe, S.H.I. (2008) An efficient strategy for gene targeting and phenotypic assessment in the *Plasmodium yoelii* rodent malaria model. *Mol Biochem Parasitol* **158:** 213–216.

Miller, J.L., Harupa, A., Kappe, S.H.I., and Mikolajczak, S.A. (2012) *Plasmodium yoelii* macrophage migration inhibitory factor is necessary for efficient liver-stage development. *Infect Immun* **80:** 1399–1407.

Mochizuki, S., Harada, A., Inada, S., Sugimoto-Shirasu, K., Stacey, N., Wada, T., *et al.* (2005) The *Arabidopsis* WAVY GROWTH 2 protein modulates root bending in response to environmental stimuli. *Plant Cell* **17:** 537–547.

Nardini, M., and Dijkstra, B.W. (1999) Alpha/beta hydrolase fold enzymes: the family keeps growing. *Curr Opin Struct Biol* **9:** 732–737.

Ollis, D.L., Cheah, E., Cygler, M., Dijkstra, B., Frolow, F., Franken, S.M., *et al.* (1992) The alpha/beta hydrolase fold. *Protein Eng* **5:** 197–211.

Pachebat, J.A., Ling, I.T., Grainger, M., Trucco, C., Howell, S., Fernandez-Reyes, D., *et al.* (2001) The 22 kDa component of the protein complex on the surface of *Plasmodium falciparum* merozoites is derived from a larger precursor, merozoite surface protein 7. *Mol Biochem Parasitol* **117:** 83–89.

Park, H.O., Bi, E., Pringle, J.R., and Herskowitz, I. (1997) Two active states of the Ras-related Bud1/Rsr1 protein bind to different effectors to determine yeast cell polarity. *Proc Natl Acad Sci USA* **94:** 4463–4468.

Parmentier, M.L., Woods, D., Greig, S., Phan, P.G., Radovic, A., Bryant, P., and O'Kane, C.J. (2000) Rapsynoid/partner of inscuteable controls asymmetric division of larval neuroblasts in *Drosophila*. *J Neurosci* **20:** RC84.

Prudencio, M., Rodriguez, A., and Mota, M.M. (2006) The silent path to thousands of merozoites: the Plasmodium liver stage. *Nat Rev Microbiol* **4:** 849–856.

Read, M., Sherwin, T., Holloway, S.P., Gull, K., and Hyde, J.E. (1993) Microtubular organization visualized by immunofluorescence microscopy during erythrocytic schizogony in *Plasmodium falciparum* and investigation of post-translational modifications of parasite tubulin. *Parasitology* **106:** 223–232.

Rosenberg, R., and Rungsiwongse, J. (1991) The number of sporozoites produced by individual malaria oocysts. *Am J Trop Med Hyg* **45:** 574–577.

Sack, B.K., Miller, J.L., Vaughan, A.M., Douglass, A., Kaushansky, A., Mikolajczak, S., *et al.* (2014) Model for *in vivo* assessment of humoral protection against malaria sporozoite challenge by passive transfer of monoclonal antibodies and immune serum. *Infect Immun* **82:** 808–817.

Schrevel, J., Asfaux-Foucher, G., Hopkins, J.M., Robert, V., Bourgouin, C., Prensier, G., and Bannister, L.H. (2008) Vesicle trafficking during sporozoite development in *Plasmodium berghei*: ultrastructural evidence for a novel trafficking mechanism. *Parasitology* **135:** 1–12.

Shortt, H.E., Fairley, N.H., Covell, G., Shute, P.G., and Garnham, P.C. (1951) The pre-erythrocytic stage of *Plasmodium falciparum*. *Trans R Soc Trop Med Hyg* **44:** 405–419.

Sinden, R.E. (1999) *Plasmodium* differentiation in the mosquito. *Parassitologia* **41:** 139–148.

Stanway, R.R., Mueller, N., Zobiak, B., Graewe, S., Froehlke, U., Zessin, P.J., *et al.* (2011) Organelle segregation into *Plasmodium* liver stage merozoites. *Cell Microbiol* **13:** 1768–1782.

Sturm, A., Amino, R., van de Sand, C., Regen, T., Retzlaff, S., Rennenberg, A., *et al.* (2006) Manipulation of host hepatocytes by the malaria parasite for delivery into liver sinusoids. *Science* **313:** 1287–1290.

Tarun, A.S., Dumpit, R.F., Camargo, N., Labaied, M., Liu, P., Takagi, A., *et al.* (2007) Protracted sterile protection with *Plasmodium yoelii* pre-erythrocytic genetically attenuated parasite malaria vaccines is independent of significant liver-stage persistence and is mediated by CD8+ T cells. *J Infect Dis* **196:** 608–616.

Tarun, A.S., Peng, X., Dumpit, R.F., Ogata, Y., Silva-Rivera, H., Camargo, N., *et al.* (2008) A combined transcriptome and proteome survey of malaria parasite liver stages. *Proc Natl Acad Sci USA* **105:** 305–310.

Thathy, V., Fujioka, H., Gantt, S., Nussenzweig, R., Nussenzweig, V., and Ménard, R. (2002) Levels of circumsporozoite protein in the *Plasmodium* oocyst determine sporozoite morphology. *EMBO J* **21:** 1586–1596.

Valencik, M.L., and Pringle, P.R. (1995) *Schizosaccharomyces pombe bem1/bud5* suppressor (*bem46*) mRNA. EMBL database, accession number U29892.

Vanderberg, J.P., and Frevert, U. (2004) Intravital microscopy demonstrating antibody-mediated immobilisation of *Plasmodium berghei* sporozoites injected into skin by mosquitoes. *Int J Parasitol* **34:** 991–996.

Vaughan, A.M., Aly, A.S.I., and Kappe, S.H.I. (2008) Malaria parasite pre-erythrocytic stage infection: gliding and hiding. *Cell Host Microbe* **4:** 209–218.

Vaughan, A.M., O'Neill, M.T., Tarun, A., Camargo, N., Phuong, T.M., Aly, A.S.I., *et al.* (2009) Type II fatty acid synthesis is essential only for malaria parasite late liver stage development. *Cell Microbiol* **11:** 506–520.

WHO (2010) *World Malaria Report: 2010*. Geneva, Switzerland: World Health Organization.

Supporting information

Additional Supporting Information may be found in the online version of this article at the publisher's web-site:

Fig. S1. Graphical representation of the putative *Plasmodium* BEM46-like protein (PBLP) open reading frame (ORF) as a genomic DNA sequence, containing 11 exons (*above*) that are processed into a single continuous mRNA transcript (*below*). Genomic DNA and RNA were isolated from *P. yoelii* 17XNL infected red blood cells (iRBCs). For the generation of cDNA, genomic DNA was removed by DNase treatment and cDNA was generated by reverse transcriptase PCR. Genomic and cDNA sequences were confirmed by sequencing (Seattle BioMed Sequencing Facility) using multiple, overlapping primers directed against the PBLP ORF. Primer sequences are available upon request.

Fig. S2. Generation of *Plasmodium yoelii pblp*-myc tag parasites. (A) Two *pblp*-myc tag parasites (*pblp*-myc #1 and *pblp*-myc #2) were designed so that the nascent PBLP ORF was replaced with a selectable drug resistance marker for positive selection (huDHFR, the human *dhfr gene*) and an ampicillin resistance (Amp) gene for bacterial selection by double-crossover homologous recombination using the 5′ UTR and 3′ UTR regions at the *pblp* locus. The resulting transgenic parasites had a 4X myc tag fused to the C-terminus of the PBLP ORF. (B) The mixed population of wild-type (WT) and transgenic parasites was cloned by serial limiting dilution into SW mice. The genotyping gel shows successful integration on the 5′ (5′ test) and 3′ (3′ test) flanks, without affecting the PBLP ORF. Additional controls included contextual reactions where the genomic sequence of both *pblp*-myc tag parasites showed complete integration of the selectable marker. Negative control was included to show lack of genomic DNA contamination in all primer pairs. (C) Reverse transcriptase PCR using primers amplifying either PBLP or 18S rRNA from WT or *pblp*-myc # 1 and *pblp*-myc #2 blood-stage parasites. RT-PCR was performed on cDNA derived from 1 μg of parasite RNA.

Fig. S3. Generation of two distinct *Plasmodium yoelii* Δ*pblp* parasites. (A) Two Δ*pblp* were designed where either short segments of the genomic DNA sequence were retained at the 5′ and 3′ ends of the open reading frame (ORF) (Δ*pblp* v1, *left*) or where the entire PBLP ORF would be removed after transfection (Δ*pblp* v2, *right*). In Δ*pblp* v1, the majority of the PBLP ORF was replaced with a selectable drug resistance marker for positive selection (tgDHFR, the *Toxoplasma gondii dhfr* gene) and a cassette encoding the green fluorescent protein (GFP) by double-crossover homologous recombination using the 5′ UTR and 3′ UTR regions at the *pblp* locus. In Δ*pblp* v2, the entire PBLP ORF was replaced with a selectable drug resistance marker for positive selection (huDHFR, the human *dhfr gene*), an ampicillin resistance (Amp) gene for bacterial selection and the cassette encoding GFP by double-crossover homologous recombination using the 5′ UTR and 3′ UTR regions at the *pblp* locus that do not include any genomic sequences. The resulting Δ*pblp* parasite populations were fluorescent green. (B) The mixed population of wild-type (WT) and transgenic parasites was cloned by serial limiting dilution into SW mice. The genotyping gel shows successful integration on the 5′ (5′ test) and 3′ (3′ test) flanks, as well as the loss of the PBLP ORF in Δ*pblp* v2 and the altered migration pattern of the PBLP ORF in Δ*pblp* v1. Additional controls included contextual reactions where the genomic sequence of both Δ*pblp* parasites (v1 and v2) showed complete integration of the selectable marker and the GFP cassette. Negative control was included to show lack of genomic DNA contamination in all primer pairs. (C) Reverse transcriptase PCR using primers amplifying either PBLP or 18S rRNA from WT or Δ*pblp* (v1 and v2) blood-stage parasites. RT-PCR was performed on cDNA derived from 1 μg of parasite RNA.

Fig. S4. Δ*pblp* parasites produce significantly less merozoites during intra-erythrocytic replication cycles, resulting in a diminished capacity to achieve wild-type (WT) replication levels *in vivo*. Blood-stage (BS) growth curves were done using 1 million WT ($n = 21$) or Δ*pblp* (v1 and v2, $n = 6$–9) mixed iRBCs, which were injected into BALB/cJ mice via IV injection. Parasitemia in the blood was measured daily until all parasites were cleared. The data are a combination of three experimental replicates. *P value ≤ 0.05.

Table S1. Putative BEM46-like protein in the *P. yoelii* 17XNL genome.